molecular pharmaceutics

Article

Cite This: Mol. Pharmaceutics 2019, 16, 1633−1647

pubs.acs.org/molecularpharmaceutics

Selective Cytotoxicity to HER2 Positive Breast Cancer Cells by Saporin-Loaded Nanobody-Targeted Polymeric Nanoparticles in Combination with Photochemical Internalization

Lucía Martínez-Jothar,[†] Nataliia Beztsinna,[†] Cornelus F. van Nostrum,[†] Wim E. Hennink,[†] and Sabrina Oliveira*[,†,‡]

[†]Department of Pharmaceutics, Utrecht Institute for Pharmaceutical Sciences, Utrecht University, Universiteitsweg 99, 3584 CG Utrecht, The Netherlands

[‡]Division of Cell Biology, Department of Biology, Utrecht University, Padualaan 8, 3584 CH Utrecht, The Netherlands

Supporting Information

ABSTRACT: In cancer treatment, polymeric nanoparticles (NPs) can serve as a vehicle for the delivery of cytotoxic proteins that have intracellular targets but that lack well-defined mechanisms for cellular internalization, such as saporin. In this work, we have prepared PEGylated poly(lactic acid-*co*-glycolic acid-*co*-hydroxymethyl glycolic acid) (PLGHMGA) NPs for the selective delivery of saporin in the cytosol of HER2 positive cancer cells. This selective uptake was achieved by decorating the surface of the NPs with the 11A4 nanobody that is specific for the HER2 receptor. Confocal microscopy observations showed rapid and extensive uptake of the targeted NPs (11A4-NPs) by HER2 positive cells (SkBr3) but not by HER2 negative cells (MDA-MB-231). This selective uptake was blocked upon preincubation of the cells with an excess of nanobody. Nontargeted NPs (Cys-NPs) were not taken up by either type of cells. Importantly, a dose-dependent cytotoxic effect was only observed on SkBr3 cells when these were treated with saporin-loaded 11A4-NPs in combination with photochemical internalization (PCI), a technique that uses a photosensitizer and local light exposure to facilitate endosomal escape of entrapped nanocarriers and biomolecules. The combined use of saporin-loaded 11A4-NPs and PCI strongly inhibited cell proliferation and decreased cell viability through induction of apoptosis. Also the cytotoxic effect could be reduced by an excess of nanobody, reinforcing the selectivity of this system. These results suggest that the combination of the targeting nanobody on the NPs with PCI are effective means to achieve selective uptake and cytotoxicity of saporin-loaded NPs.

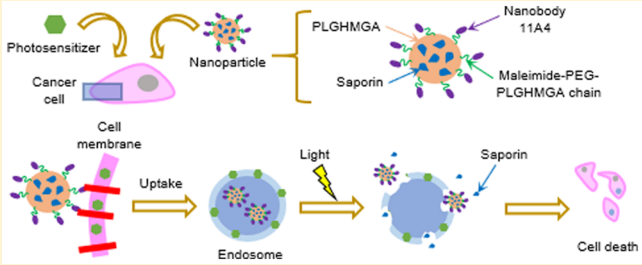

KEYWORDS: *nanobody, targeting, polymeric nanoparticles, photochemical internalization, saporin, PLGA*

1. INTRODUCTION

Proteins are widely recognized as valuable therapeutic agents because of their high potency and target specificity. A large number of the currently approved therapeutic proteins is indicated for cancer therapy, one of the leading causes of death worldwide, as classic low molecular weight chemotherapeutic drugs result in substantial off-target toxicity.[1]

In the search for new antineoplastic drugs, the ribosome-inactivating protein (RIP) saporin (from the plant *Saponaria officinalis*) has emerged as an agent of interest because of its potent cytotoxic effect, stability at high temperature, resistance to denaturation, and ease of chemical modification.[2,3] Several cytotoxic mechanisms have been described for saporin, including inhibition of protein synthesis, DNA-fragmentation, and induction of apoptosis via the intrinsic and extrinsic pathways.[4−7] Saporin is a type I RIP, and unlike type II RIPs, it lacks the galactose-specific lectin that mediates cell binding and entrance. It has been reported that saporin can enter some cells via endocytosis mediated by the α_2-macroglobulin receptor[8] or by receptor-independent mechanisms.[9] However, the mechanism of internalization of saporin is not yet completely clear, and alternatives have been developed in order to achieve enhanced, cell-specific uptake of this protein to increase its cytotoxicity. Particularly, saporin−antibody conjugates (immunotoxins) have been commonly used for this purpose.[10−13] While immunotoxins have shown promising efficacy *in vitro* and *in vivo*, their use in clinical settings has been mostly limited by their immunogenicity and induction of vascular leak syndrome.[14,15] Furthermore, the preparation of immunotoxins often requires conjugation strategies to chemically link the toxin to the antibody.

The use of nanocarriers is another approach for the efficient intracellular delivery of saporin[16−19] and other biotherapeutics

Received: December 20, 2018
Revised: February 13, 2019
Accepted: February 28, 2019
Published: February 28, 2019

with limited membrane permeability (proteins and nuclei acid based drugs).[20−22] In particular, polymeric nanoparticles (NPs) have attracted increasing attention as nanocarriers over the past 20 years due to their ability to increase the physicochemical stability of their cargo and provide certain control over when, where, and how it is released, thus improving its pharmacokinetic and pharmacodynamic profiles.[23,24] In the present study, NPs made from PEGylated poly(lactic acid-*co*-glycolic acid-*co*-hydroxymethyl glycolic acid) (PLGHMGA) were used for the encapsulation and delivery of saporin. PLGHMGA is structurally related to poly(lactic-*co*-glycolic acid) (PLGA), though it contains pending hydroxyl groups that increase its hydrophilicity and shorten its degradation time.[25] Encapsulation of a peptide in PLGHMGA microparticles resulted in less chemical modifications (acylation) than in PLGA microparticles,[26,27] which points to an improved compatibility of PLGHMGA with biomolecules and suggests that PLGHMGA NPs could be a suitable nanocarrier for saporin.

The efficiency and selectivity of polymeric NPs as nanocarriers can be further increased by functionalization of their surface with targeting ligands that bind to cell surface receptors overexpressed in tumors.[28−31] Nanobodies, also known as VHHs, are variable domains of the heavy chain of heavy chain antibodies present in camelids,[32] and they are the smallest naturally occurring antigen binding fragments. The structure and small size of nanobodies (∼15 kDa) confers them advantages over conventional antibodies or fragments thereof, including an increased solubility and stability, less propensity for aggregation, easier production, and greater ability to reach and neutralize targets that are not easily accessible.[33,34] Furthermore, nanobodies display low immunogenicity because of their high sequence homology with the VH of human antibodies,[35] and if needed, additional homology can be easily obtained by humanization of specific residues without detrimental effects on their stability and affinity.[36] Importantly, nanobodies can selectively target a variety of receptors, including HER2 (Human Epidermal Growth Factor Receptor 2), which is overexpressed in several types of malignancies such as breast, gastric, lung, and ovarian cancers, and is associated with poor prognosis.[37,38] The nanobody 11A4 binds specifically to the HER2 receptor with high affinity and has shown promise for optical imaging of breast cancer *in vivo*[39,40] and for immunolabeling of HER2 for electron microscopy.[41] Nanobodies targeting the HER2 receptor, as well as other receptors such as the epidermal growth factor receptor (EGFR) and the hepatocyte growth factor receptor (HGFR), have been used in the field of drug delivery for the functionalization of liposomes,[42,43] polymeric micelles,[44,45] albumin nanoparticles,[46,47] and polymersomes,[48] resulting in selective and efficient receptor-mediated uptake of these systems. In the present work, the targeting properties of the nanobody 11A4 were explored to achieve enhanced and selective uptake of polymeric NPs by HER2 overexpressing breast cancer cells.

Upon ligand−receptor interaction, polymeric NPs are internalized by endocytosis and can therefore act as intracellular delivery systems. However, those NPs are then inside endocytic vesicles, which later fuse with lysosomes.[49] Thus, to prevent cargo molecules such as proteins from being degraded, strategies have been developed for endosomal escape of nanocarriers and/or their cargo. Release of the NPs from the endosome can be accomplished either by nanoparticle design (incorporation of elements for proton sponge effect, membrane disruption, or pore formation)[50−52] or by means of external stimuli, such as photochemical internalization (PCI). This technique makes use of an amphiphilic photosensitizer (PS), which localizes in the cell membrane and, upon endocytosis of the NPs, becomes a part of the endosomal membrane where the NPs are entrapped. Upon excitation with light of the appropriate wavelength, the PS will produce reactive oxygen species that damage the endosomal membrane, which results in destabilization of this membrane and subsequently in release of its contents into the cytosol.[53] PCI has been successfully used both *in vitro* and *in vivo* for the delivery of proteins, immunotoxins, chemotherapeutics, genetic material, and nanocarriers.[54−56] Importantly, phase I clinical trials have proven the safety and tolerability of the PS disulfonated tetraphenyl chlorin ($TPCS_{2a}$) used for PCI of bleomycin for the treatment of cutaneous and subcutaneous malignancies.[57] Additionally, a phase I/II clinical trial involving PCI of gemcitabine for the treatment of cholangiocarcinomas is currently underway.[58]

In the present work, the potency and selectivity of a new formulation was investigated, combined with PCI, to assess its capacity to locally deliver a cytotoxic molecule to target cells. For this purpose, PEG−PLGHMGA NPs loaded with saporin and functionalized with the 11A4 nanobody were prepared and characterized. The uptake of these NPs was investigated, and their cytotoxicity was evaluated in combination with PCI in both HER2 positive and negative breast cancer cell lines. The contribution of each one of the elements under study to the cytotoxicity of the treatment was also evaluated.

2. EXPERIMENTAL SECTION

2.1. Materials. D,L-Lactide was obtained from Corbion (Gorinchem, The Netherlands). BMG, a dilactone containing a protected benzyl group, was synthesized as described previously.[59] Benzyl alcohol, tin(II) 2-ethylhexanoate, poly(vinyl alcohol) (PVA; M_w 30 000−70 000 Da (87−90% hydrolyzed)), and L-cysteine hydrochloride monohydrate were purchased from Sigma-Aldrich (Steinheim, Germany). Poly(ethylene glycol) monomethyl ether ($M_n \approx 2000$ Da) and palladium on carbon (10 wt % loading) were acquired from Aldrich (Steinheim, Germany). Poly(lactic-*co*-glycolic)-cysteine ethyl ester (PLGA-SH, M_w 30 000 Da) and poly(lactide-*co*-glycolide)-*b*-poly(ethylene glycol)-maleimide (maleimide−PEG-PLGA, M_w 5000/20 000 Da) were purchased from Polyscitech, Akina Inc. (Indiana, USA). Micro BCA Protein Assay Kit and Pierce Silver Stain Kit were purchased from Thermo Scientific (Illinois, USA). Alexa-568 C5 maleimide was obtained from Thermo Fisher Scientific (Oregon, USA). Saporin from *Saponaria officinalis* seeds (as a lyophilized powder containing protein, glucose, and sodium phosphate buffer salts), Dulbecco's phosphate buffered saline (8.0 g of NaCl, 1.15 g of Na_2HPO_4, 0.2 g of KCl, and 0.2 g of KH_2PO_4 in 1 L of water, pH 7.4), McCoy's 5A medium, Dulbecco's modified Eagle's medium (DMEM)-high glucose, fetal bovine serum, antibiotic antimycotic solution (10,000 units of penicillin, 10 mg of streptomycin, and 25 μg of amphotericin B/mL), resazurin sodium salt, staurosporine from *Streptomyces* sp., and Triton X-100 were purchased from Sigma (Steinheim, Germany). The PS meso-tetraphenyl porphyrin disulfonate ($TPPS_{2a}$)[60] was kindly provided by Dr. Anders Høgset (PCI Biotech, Oslo, Norway). The BrdU assay kit was acquired from Roche (Manheim, Germany). Annexin V-FITC (90 μg/mL) was purchased from Biolegend (California, USA). Propidium iodide (1.0 mg/mL) was acquired from Invitrogen (Oregon, USA).

DOI: 10.1021/acs.molpharmaceut.8b01318
Mol. Pharmaceutics 2019, 16, 1633−1647

2.2. Synthesis of Poly(D,L-lactic-*co*-glycolic-*co*-hydroxymethyl glycolic acid) (PLGHMGA) and Methoxy−PEG−PLGHMGA (MePEG−PLGHMGA). Poly(D,L-lactic-*co*-glycolic-*co*-benzyloxymethyl glycolic acid) (PLGBMGA) was synthesized by copolymerization of D,L-lactide and benzyloxymethyl glycolide (BMG) in the melt at a ratio of 65:35 mol/mol %. Benzyl alcohol was used as initiator at a 300:1 monomer to initiator molar ratio, and the catalyst tin(II) 2-ethylhexanoate was employed at a 2:1 molar ratio of initiator to catalyst as reported elsewhere.[61] The protecting benzyl groups of the polymer were removed by hydrogenation catalyzed by palladium on carbon following a previously described protocol.[59] The resulting polymer, PLGHMGA, was purified by precipitation in cold diethyl ether, recovered by filtration, and dried under vacuum.

MePEG−PLGHMGA was prepared as described for PLGHMGA, but poly(ethylene glycol) monomethyl ether was used as an initiator instead of benzyl alcohol.[61]

2.3. Polymer Characterization. The composition of PLGHMGA was determined by ^{1}H NMR in deuterated DMSO. The molar % of lactic acid (L), glycolic acid (G), and hydroxymethyl glycolic acid (HMG) was calculated based on the peak integrals (I_{ppm}) of the monomers,[61] as follows:

$$I_L = [(I_{5.1-5.4}) - (I_{3.6-3.9}/2)]$$

$$I_G = (I_{4.7-5.0})/2$$

$$I_{HMG} = [(I_{3.6-3.9}/2) + (I_{4.1-4.5}/3)]$$

$$\%_L = I_L/(I_L + I_G + I_{HMG}) \times 100$$

$$\%_G = I_G/(I_L + I_G + I_{HMG}) \times 100$$

$$\%_{HMG} = I_{HMG}/(I_L + I_G + I_{HMG}) \times 100$$

The % PEG in MePEG−PLGHMGA was also determined based on ^{1}H NMR analysis[61] as follows:

$$\text{calculated polymer Mn} = [(I_L/I_{PEG} \times \text{Mw L unit}) + (I_G/I_{PEG} \times \text{Mw G unit}) + (I_{HMG}/I_{PEG} \times \text{HMG unit})] + \text{PEG Mw}$$

$$\%_{PEG} = \text{PEG Mw/calculated polymer Mn} \times 100$$

The molecular weights of the polymers were determined by gel permeation chromatography (GPC) (Waters 2695 separating module and Waters 2414 refractive index detector) using two PL-gel 5 μm Mixed-D columns and tetrahydrofuran as the mobile phase (1 mL/min) at 60 °C. Polystyrene standards (EasiCal Agilent, California, USA) and PEG standards were used for calibration.

The thermal properties of the polymers were studied using differential scanning calorimetry (Discovery DSC, TA Instruments, Delaware, USA). Briefly, a sample of ∼5 mg of polymer was transferred into an aluminum pan and heated from room temperature to 120 °C at a rate of 5 °C/min and subsequently cooled down to −50 °C at the same rate. The polymer was then heated to 120 °C at a rate of 2 °C/min with temperature modulation at ±1 °C.

2.4. Synthesis of Alexa-568-PLGA. Fluorescently-labeled PLGA was prepared by maleimide−thiol reaction of PLGA-SH (thiol end-cap) and Alexa-568 C5 maleimide at an equimolar ratio.[62] Briefly, PLGA-SH was dissolved in acetonitrile (25 mg/mL), and Alexa-568 C5 maleimide was dissolved in PBS/EDTA 4 mM (10 mg/mL, pH 7.4). The Alexa dye (0.1 mL) was added to PLGA-SH (1 mL), and the mixture was stirred in the dark at room temperature for 2 h. The polymer was recovered by precipitation in cold methanol followed by centrifugation (20 min, 20 000*g*, 4 °C). The polymer pellet was recovered and dried under reduced pressure.

2.5. Polymeric Nanoparticles (NPs) Preparation and Characterization. The NPs were prepared using a double emulsion solvent evaporation method,[61,63,64] starting from a mixture of PLGHMGA, MePEG−PLGHMGA, and maleimide−PEG-PLGA in a 8:1:1 w/w ratio. For the preparation of fluorescent particles, 2% w/w of Alexa-568-PLGA was added to the polymer mixture. The polymers were dissolved in dichloromethane at 5% w/v and 200 μL of an aqueous solution of saporin (5 mg protein/mL) or 200 μL of water (for preparation of placebo NPs) were added to 1 mL of this polymer solution. The mixture was subsequently emulsified for 1 min at 20 W power using a probe sonicator (SONOPULS HD 2200 Bandelin, Berlin, Germany) in an ice bath. Next, this W/O emulsion was added dropwise to 10 mL of an aqueous solution of PVA 5% w/v and NaCl 0.9% w/v. The addition was done while sonicating the sample in an ice bath for 2 min at 20 W power. The resulting W/O/W emulsion was stirred at 600 rpm for 2 h at room temperature to evaporate the dichloromethane. Subsequently, the NPs were collected by centrifugation for 20 min, 20 000*g* at 4 °C, and washed with PBS and UltraPure distilled water (Invitrogen, Paisley, UK). After the second washing, the NPs were resuspended in 1 mL of UltraPure distilled water and divided into aliquots of equal volume (200 μL). One of the aliquots was freeze-dried at −40 °C, <1 mbar (Christ Alpha 1−2 freeze-dryer) and used to determine the yield of the NPs and their protein content (section 2.6). The other aliquots were supplemented with sucrose at a final concentration of 5% w/v and freeze-dried at −40 °C, <1 mbar.

The diameter of the different NPs was determined by dynamic light scattering (Zetasizer Nano S, Malvern, Worcestershire, UK) at 25 °C in Milli-Q water (the concentration of the suspension was 100 μg NPs/mL), and their zeta potential (Zetasizer Nano Z, Malvern, Worcestershire, UK) was measured at 25 °C in HEPES 10 mM pH 7.0 (100 μg NPs/mL).

2.6. Determination of Saporin Loading of the NPs. The saporin encapsulation efficiency of the NPs was determined by a previously described method.[65] In short, 5 mg of freeze-dried NPs was degraded in 3 mL of a solution of 0.05 M NaOH containing 0.5% w/v of sodium dodecyl sulfate at 37 °C for 2 h. The protein content in the resulting solution was determined by MicroBCA Assay (according to the specifications of the manufacturer). A sample of saporin was treated in the same way as the NPs and for calibration in the range of 2−40 μg/mL. The encapsulation efficiency and loading capacity were calculated as follows:

$$\text{encapsulation efficiency \%} = \frac{\text{amount of protein trapped}}{\text{amount of protein used in preparation}} \times 100$$

$$\text{loading \%} = \frac{\text{amount of protein trapped}}{\text{dry weight of NPs used in the test}} \times 100$$

2.7. *In Vitro* Release of Saporin from the NPs. Freeze-dried saporin-loaded NPs were suspended at a concentration of 5 mg/mL in PBS. The NPs suspension was divided into aliquots

DOI: 10.1021/acs.molpharmaceut.8b01318
Mol. Pharmaceutics 2019, 16, 1633−1647

of 300 μL, which were incubated at 37 °C under mild agitation. At different time points, an aliquot was taken and centrifuged for 10 min, 20 000*g* at 4 °C and the supernatant (containing the released saporin) was collected and stored at −20 °C until the end of the study. The supernatants were analyzed by SDS-PAGE under reducing conditions: 30 μL of the supernatants was diluted with 10 μL of sample buffer (8% w/v SDS, 40% v/v glycerol, 0.008% w/v bromophenol blue, 20% v/v 2-mercaptoethanol in buffer Tris-HCl pH 6.8), and 20 μL of the diluted sample was loaded into a Bolt 4−12% Bis-Tris Plus gel (Invitrogen, California, USA). The same procedure was followed for standards containing known amounts of saporin (2−8 ng/ μL). The protein in the gel was visualized by silver staining (performed according to the instructions of the manufacturer). The gel was imaged using a ChemiDoc MP imager (Bio-Rad, California, USA) and analyzed with ImageJ software (NIH, USA). The gel analysis function on ImageJ was used to generate plots from the intensity of the pixels in a selected area (area of the protein band). The amount of saporin in the release samples was calculated by comparing the peak areas of the plots to the peak areas from the standards.

2.8. Conjugation of 11A4 Nanobody to the NPs. The 11A4 nanobody containing a C-terminal cysteine (theoretical M_w 14 813 Da by ExPASy ProtParam) was produced and purified, as previously described.[39,40] The conjugation reaction was conducted according to our previous study.[66] In short, an amount of freeze-dried NPs was resuspended in water and pelleted by centrifugation (10 min, 3000*g* at 4 °C). Subsequently, the NP pellet was resuspended in PBS/EDTA 0.4 mM to a concentration of ∼3.5 mg NPs/mL and mixed with the nanobody at a molar ratio of 10:1 maleimide−PEG-PLGA to nanobody. The samples were incubated for 2 h at room temperature on a nutating mixer. Subsequently, the non-conjugated nanobody was separated from the 11A4 functionalized NPs (11A4-NPs) by centrifugation and quantified by UPLC.[66] The conjugation efficiency was determined as

$$\text{conjugation efficiency \%} = \left(1 - \left(\frac{[\text{ligand in the supernatant}]}{[\text{ligand added in the conjugation reaction}]}\right)\right) \times 100$$

The same protocol was used to prepare control NPs in which the maleimide groups were blocked with cysteine (Cys-NPs) with two differences: the molar ratio of the reactants was 1:2 maleimide−PEG-PLGA to cysteine and the nonconjugated cysteine was quantified by MicroBCA Assay, as described by the provider.

2.9. Cell Lines and Culture Conditions. Human breast cancer cell lines SkBr3 (HER2 positive, ATCC HTB-30) and MDA-MB-231 (HER2 negative, ATCC CRM-HTB-26) were obtained from American Type Culture Collection (Virginia, USA). Mycoplasma tests were performed regularly on the cells in culture. SkBr3 cells were cultured in McCoy's 5A medium, supplemented with 10% fetal bovine serum, while MDA-MB-231 cells were maintained in Dulbecco's modified Eagle's medium (DMEM)-high glucose with 10% fetal bovine serum. The cells were incubated at 37 °C in a humidified atmosphere containing 5% CO_2. These conditions were also used in all cell incubation steps in the experiments described below.

2.10. Cellular Uptake of NPs. SkBr3 or MDA-MB-231 cells were seeded at a density of 10,000 cells/well in 96-well μClear black plates (Greiner Bio-One, Frickenhausen, Germany). The cell nuclei were stained with 10 nM Hoechst 33342 in PBS for 10 min at 37 °C, and after washing off the excess of dye, fresh medium was added to the cells. The cells were incubated with placebo 11A4-NPs or with Cys-NPs, both labeled with Alexa-568 at 37 °C. The NPs concentration in the wells was 22 μg/mL. In order to study the uptake kinetics of NPs, confocal microscopy of living cells was conducted using a Yokogawa CV7000s high-content imager (Yokogawa Electric Corporation, Tokyo, Japan). Cells were kept at 37 °C, in a humidified atmosphere with 5% CO_2 during the imaging process, and confocal images through the middle plane of the cells were taken 15 min, 30 min, 1 h, 2 h, 4 h, 6 h, and 8 h after the addition of the NPs to the cells. Images were captured in two channels: Hoechst 33342 for nuclei (λ_{ex} 405 nm, λ_{em} 445 nm) and Alexa-568 to visualize the NPs (λ_{ex} 561 nm, λ_{em} 600 nm). The image analysis was performed with the Columbus Image Data Storage and Analysis System (PerkinElmer). The reported values are the mean and SD of the data obtained from three wells containing five imaging fields each.

To investigate whether the uptake occurred via the HER2 receptor, competition experiments were conducted with an excess of 11A4 present in the medium. To this end, cells were preincubated with free 11A4 nanobody at a concentration of 12 μg/mL for 30 min, followed by the addition of the Alexa-568 labeled placebo NPs functionalized with the 11A4 nanobody, at a final concentration of 80 μg/mL. Consequently, there was a 55-fold molar excess of free 11A4 nanobody compared to the 11A4 conjugated to the NPs. After 30 min of incubation, the medium (containing free 11A4 and the 11A4-NPs) was removed, the cells were washed with PBS, and fresh medium was added. Confocal microscopy of living cells was conducted as described above and including phase contrast imaging to better delineate the cell membrane.

2.11. Photochemical Internalization (PCI). PCI was conducted using the PS $TPPS_{2a}$, which was dissolved in dimethyl sulfoxide at a concentration of 1 mg/mL, aliquoted, and stored at −20 °C. The samples containing PS were handled under dim light and incubated in the dark. The PCI experiments were conducted on cells seeded at a density of 5000 cells/well on 96-well plates (100 μL of cell suspension per well), after overnight culture, as described previously:[54,67] $TPPS_{2a}$ was diluted in cell culture medium supplemented with antibiotics (1200 units penicillin, 1.2 mg of streptomycin, and 3 μg of amphotericin B/mL) to a concentration of 6 μg/mL. Next, 10 μL of this solution was added per well, and the cells were incubated for 14 h. Subsequently, 10 μL of a suspension of placebo NPs or saporin-loaded NPs in cell culture medium was added per well (NPs concentrations for each experiment are given in sections 2.13 and 2.14). The cells were incubated with the PS and the NPs for 4 h (total incubation time with the PS was therefore 18 h), followed by removal of the medium and addition of fresh medium containing antibiotics (100 units of penicillin, 0.1 mg of streptomycin, and 0.25 μg of amphotericin B/mL). The cells were incubated with fresh medium for an additional 4 h (to favor removal of the PS from the cell membrane),[68] and subsequently, the plate was illuminated for 40 s at 420 nm using a LumiSource blue light lamp (PCI Biotech, Oslo, Norway), with an irradiance of ∼13.5 mW/cm^2 (corresponding to a total light dose of ∼0.5 J/cm^2). After illumination, the cells were incubated for 40 h without medium refreshment and then subjected to viability or proliferation assays (section 2.13).

DOI: 10.1021/acs.molpharmaceut.8b01318
Mol. Pharmaceutics 2019, 16, 1633−1647

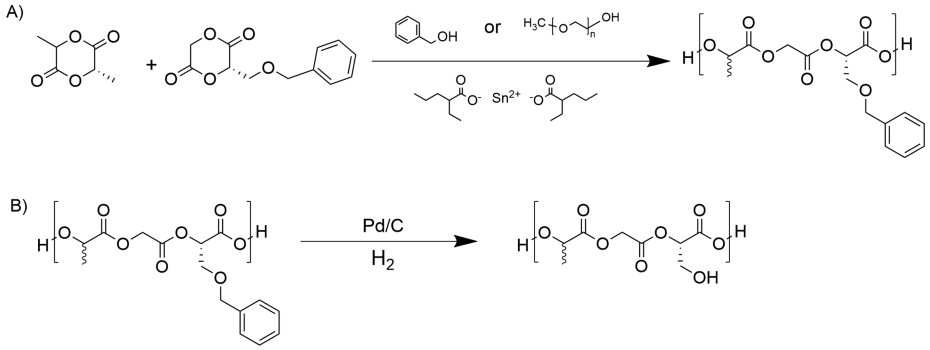

Figure 1. Synthesis of PLGHMGA. (A) Copolymerization of D,L-lactide and BMG results in the formation of PLGBMGA. (B) Removal of the protecting benzyl groups yields PLGHMGA.

2.12. Cytotoxic Effect of PCI. The cytotoxic effect of PCI, also referred to as photochemical cytotoxicity, was evaluated as follows: SkBr3 and MDA-MB-231 cells were seeded at a density of 5000 cells/well on 96-well plates. After overnight culture, 10 μL of a $TPPS_{2a}$ solution (6 μg/mL) were added per well, followed by incubation of the cells with the PS for 18 h. Next, the medium was removed and replaced with fresh medium containing antibiotics (100 units of penicillin, 0.1 mg of streptomycin, and 0.25 μg of amphotericin B/mL, Sigma). The cells were incubated for an additional 4 h, and subsequently, the plate was illuminated for 20, 40, and 60 s at 420 nm with an irradiance of ~13.5 mW/cm^2, corresponding to a total light dose of ~0.3, 0.5, and 0.8 J/cm^2. The cells were subjected to viability and proliferation assays (section 2.13) 40 h after illumination.

2.13. Cytotoxicity of the NPs. SkBr3 or MDA-MB-231 cells were seeded at a density of 5000 cells/well on 96-well plates and incubated overnight, after which they were subjected to PCI as described in section 2.11 (briefly, 14 h incubation with $TPPS_{2a}$ and 4 h incubation with PS and NPs, then 4 h incubation with fresh medium and subsequent illumination). Placebo or saporin-loaded NPs, functionalized with 11A4 or cysteine (11A4-NPs or Cys-NPs, section 2.8), were used. The final NP concentration in the wells ranged from 0.3 to 180 μg/mL and was slightly adjusted between NPs batches in order to have total saporin concentrations ranging from 0.1 to 32 nM based on the saporin loading studies in section 2.6. These concentration ranges correspond to 0.01 to 4.2 nM of saporin based on the *in vitro* release (section 2.7) for the time frame of the study. The cell viability and cell proliferation were assessed 40 h after the cells were illuminated for PCI. Cell viability was determined using resazurin, a weakly fluorescent dye that can be reduced to a fluorescent product (resorufin) by metabolically active cells.[69] In short, 10 μL of a 500 mM solution of resazurin was added to each well, and after 4 h of incubation, the fluorescent signal was measured at 530 nm excitation/600 nm emission in a multimode microplate reader Mithras LB 940 (Berthold Technologies, Bad Wildbad, Germany). Cell proliferation was determined by BrdU assay (according to the instructions of the manufacturer). The EC_{50} value of the NPs was determined by analysis of the cell proliferation data (respective to a control exposed to PCI without protein and NPs) with the software GraphPad Prism 7 (GraphPad, California, USA) (nonlinear regression, log-[inhibitor] vs normalized response−variable slope).

To investigate that the HER2 mediated uptake is essential for the cytotoxic effect, competition experiments were conducted on SkBr3 cells: after 14 h incubation with the PS, the cells were incubated with the PS and free 11A4 nanobody at a concentration of 12 μg/mL for 30 min. Subsequently, saporin-loaded NPs functionalized with the 11A4 nanobody were added to the cells at a final concentration of 80 μg/mL. The cells were incubated with the PS and the NPs for 4 h at 37 °C (total incubation time with the PS was therefore 18 h). Next, the cells were irradiated as described in section 2.11, and cell viability and cell proliferation were evaluated.

Dose−response assays were also conducted using free saporin. In short, the same protocol described for the dose−response assays of the NPs was followed, but the cells were incubated with saporin instead of NPs. The final saporin concentration in the wells ranged from 0.002 to 200 nM (6×10^{-5} to 6 μg/mL).

2.14. Apoptosis Assay. SkBr3 cells were seeded at a density of 5000 cells/well in 96-well plates, incubated overnight, and subjected to PCI as described in section 2.11. The cells were incubated with saporin-loaded NPs functionalized with 11A4 nanobody or with cysteine (control formulation) at a final concentration of 90 μg/mL. After illumination, the cells were incubated for 40 or 120 h without medium refreshment and then subjected to the apoptosis assay according to the instructions of the manufacturer. Briefly, the medium was replaced with a solution containing PI diluted 1:1000 and Annexin V-FITC diluted 1:80 in McCoy's 5A cell culture medium supplemented with 10% fetal bovine serum. Cells exposed to 10 μM staurosporine overnight were used as a positive control for apoptosis. Alternatively, cells incubated for 15 min with 1% Triton X-100 were used as positive controls for necrosis.[70] Thereafter and in both cases, the medium was replaced with the Annexin V/PI solution. After incubation for 10 min at 37 °C with the Annexin V and PI, the cells were imaged with an EVOS microscope (Thermo Fischer Scientific, Bleiswijk, The Netherlands) using the bright field, GFP (for Annexin V), and Texas Red (for PI) channels. The images were analyzed with the ImageJ software (NIH, USA) (mean gray value measurements).

2.15. Statistical Analysis. Statistical significance was evaluated using the unequal variance *t* test for comparison of the cytotoxicity of Cys-NPs + PCI vs 11A4-NPs + PCI (at different concentrations of NPs), and for the comparison of the cytotoxicity of 11A4-NPs + PCI vs 11A4 + 11A4-NPs + PCI. A value of $p \leq 0.05$ was considered significant. Statistical significance was depicted as $^*p \leq 0.05$ and $^{**}p \leq 0.01$.

3. RESULTS AND DISCUSSION

The potent cytotoxic effect of saporin makes it a promising anticancer agent. Nevertheless, the mechanism of internalization of this protein varies among cell types and is not yet clearly

DOI: 10.1021/acs.molpharmaceut.8b01318
Mol. Pharmaceutics 2019, 16, 1633−1647

understood.[8,9,71] In the present work, we encapsulated saporin in PEG−PLGHMGA NPs functionalized with the nanobody 11A4 to favor uptake and cell-specific toxicity in HER2 overexpressing cancer cells. As receptor-mediated uptake of NPs can lead to lysosomal degradation of their contents, PCI was employed to promote endosomal escape and to guarantee the release of saporin into the cytosol, where it can ultimately exert its cytotoxic effect.

3.1. Characterization of the Polymers PLGHMGA and MePEG−PLGHMGA. The polymers used in this study were synthesized by ring opening polymerization of D,L-lactide and BMG using benzyl alcohol as initiator for PLGHMGA and poly(ethylene glycol) monomethyl ether as initiator for MePEG−PLGHMGA, and tin(II) 2-ethylhexanoate as catalyst for both polymers[61] (Figure 1).

Table 1. Characteristics of the Polymers Prepared for This Study

	PLGBMGA	PLGHMGA	MePEG−PLGBMGA	MePEG−PLGHMGA
composition ratio a/b[a]				
^{1}H NMR	40:60	40:60	41:59	45:55
yield (%)	94	71	98	53
molecular weight (kDa)				
M_n (GPC)	59	43	28	22
M_w (GPC)	89	62	43	31
PDI (GPC)	1.50	1.47	1.52	1.42
M_n (^{1}H NMR)	NA[b]	NA[b]	55	83
M_n (expected)	53	43	55	45
MePEG (w%)	NA[b]	NA[b]	3.6	2.4
T_g (°C)	32	56	26	48

[a]a/b represents the molar ratio of BMG/D,L-lactide or HMG/D,L-lactide. Monomer feed was 35(a):65(b). Monomer to initiator ratios were 300:1. [b]Not applicable.

The synthesized polymers were analyzed by ^{1}H NMR, GPC, and DSC (Table 1). The polymer composition as determined by ^{1}H NMR was, within the experimental error, close to the feed ratio. The molecular weight of the polymers determined by GPC only slightly decreased after deprotection indicating that no chain scission had occurred. The molecular weight of MePEG−PLGHMGA calculated by ^{1}H NMR increased after deprotection, which might be ascribed to hydrolysis of the ester bond that connects the PEG and the PLGHMGA block during deprotection and/or subsequent purification. According to DSC analysis, the polymers were completely amorphous (Figure S1) and their T_g is consistent with previous reports.[61]

The structure and ^{1}H NMR spectra of PLGHMGA and MePEG−PLGHMGA are presented in Figure S2. The absence of a peak at 7.3 ppm confirmed that the benzyl groups were successfully removed from the polymers by hydrogenolysis (Figure S3), which resulted in pending hydroxyl groups on the polymer chain.

3.2. Preparation and Characterization of the Polymeric NPs. Placebo and saporin-loaded NPs were prepared using a blend of PLGHMGA, MePEG−PLGHMGA, and maleimide−PEG-PLGA. To prepare fluorescent NPs, PLGA-Alexa-568 was also added to the aforementioned polymer mixture. HER2 targeted NPs were prepared by conjugating the nanobody 11A4 (containing a C-terminal cysteine) to the nanoparticle surface, i.e., 11A4-NPs, exploiting the maleimide−thiol reaction. In the nontargeted NPs, cysteine was used to block the maleimide groups, i.e., Cys-NPs, because free maleimide groups can interact with cellular thiols and lead to enhanced, nonspecific cellular uptake.[72,73] The physicochemical properties of the NPs used in this study are displayed in Table 2.

For all formulations tested (NPs, Cys-NPs, and 11A4-NPs) the surface charge of saporin-loaded NPs (formulations 4−6) was closer to neutrality than the charge of placebo NPs (formulations 1−3 and 7−9). Since saporin has an isoelectric point of ∼9.4 (ExPASy ProtParam tool), the protein will carry a net positive charge at neutral pH. The less negative zeta potential of the saporin-loaded NPs can therefore be explained by the presence of surface-associated saporin.[74,75] Since saporin lacks free thiol groups in its sequence (UniProtKB) its association to the NPs is not a result of conjugation to maleimide.

The Cys-NPs (formulations 2 and 5) had similar size and surface charge to the placebo NPs without surface decoration (formulations 1 and 4). However, 11A4-NPs (formulations 3 and 6) were larger and displayed a more negative surface charge than the nondecorated NPs. Based on the isoelectric point of the nanobody 11A4 (∼7.9 according to ExPASy ProtParam tool), a slightly positive charge of 11A4-NPs would be expected at the pH conditions used for their preparation and analysis (pH 7.4). Nevertheless, the isoelectric point refers to the charge of the protein determined by its primary structure, while the folded protein can carry a different charge, depending on the amino acids located on its surface. In the case of 11A4-NPs, the zeta

Table 2. Size, Zeta Potential, and Conjugation Efficiency of Polymeric NPs

formulation	yield (%)	code	ligand	diameter (nm)[a]	PDI[b]	Zeta potential (mV)	Conjugation efficiency (%)[c]	11A4 molecules per NP[d]
placebo NPs[e]		1	none	369 ± 46	0.32	−7.1 ± 0.9	NA[f]	
	55 ± 5	2	Cys	374 ± 34	0.22	−8.2 ± 1.2	58 ± 1	
		3	11A4	435 ± 32	0.27	−11.7 ± 0.8	55 ± 7	∼7100
saporin-loaded NPs[e]		4	none	344 ± 12	0.17	−3.3 ± 0.6	NA[f]	
	55 ± 2	5	Cys	375 ± 11	0.12	−3.6 ± 0.6	61 ± 4	
		6	11A4	414 ± 26	0.16	−4.0 ± 0.8	31 ± 4	∼3400
fluorescent placebo NPs[g]		7	none	ND[h]	ND[h]	−8.5	NA[f]	
	49	8	Cys	405	0.23	−7.4	58	
		9	11A4	445	0.31	−12.8	46	∼6300

[a]Diameter of freeze-dried NPs after resuspension in PBS/EDTA 0.4 mM and conjugation with different ligands. [b]SD ≤ 0.1. [c]Conjugation efficiency % = (1 − ([ligand in the supernatant]/[ligand added in the conjugation reaction])) × 100. [d]Calculated as reported in ref 66. [e]n = 3. [f]Not applicable. [g]n = 1. [h]Not determined.

DOI: 10.1021/acs.molpharmaceut.8b01318
Mol. Pharmaceutics 2019, 16, 1633−1647

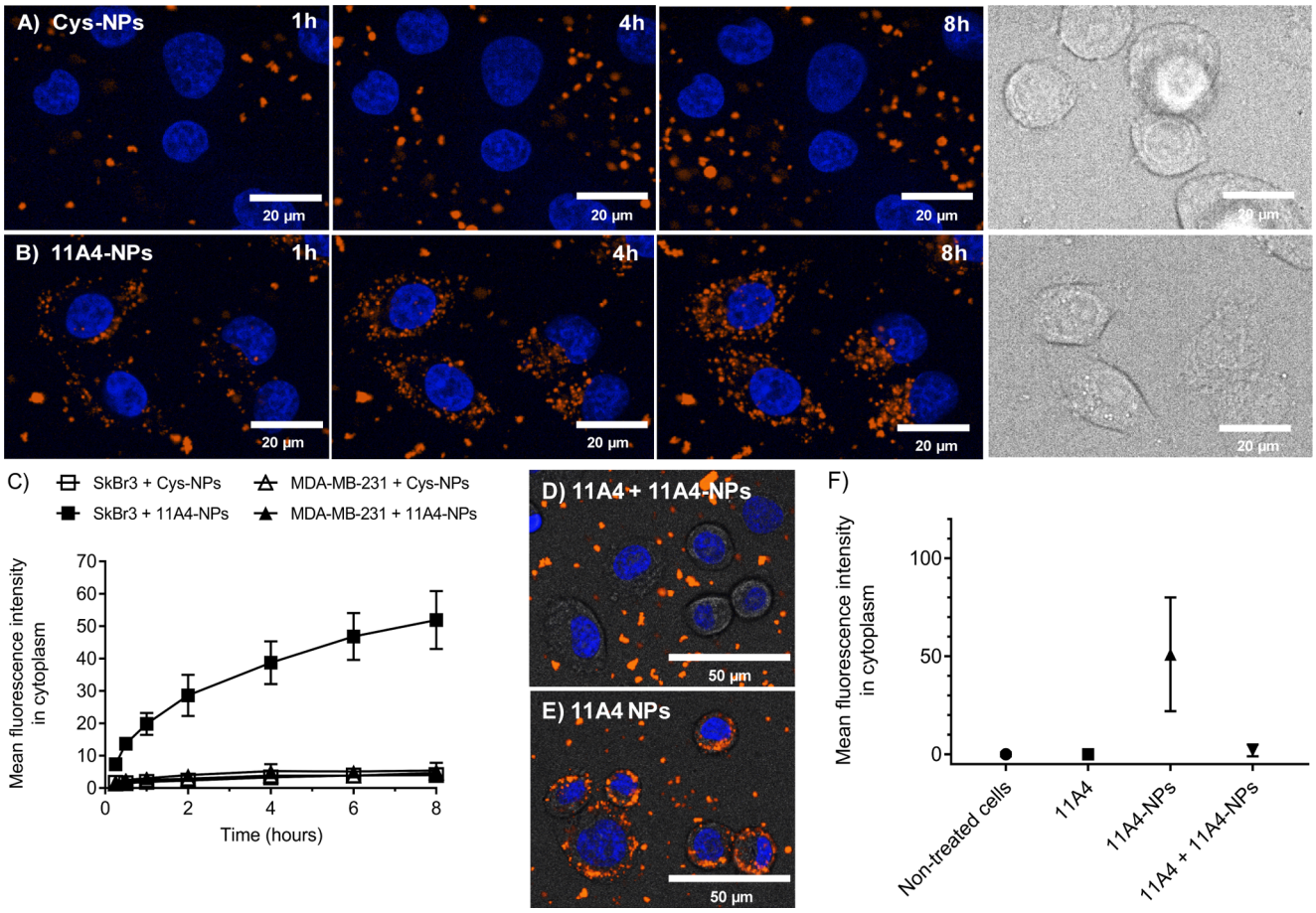

Figure 2. Cellular uptake of fluorescently labeled, targeted, and nontargeted placebo NPs. Confocal images of SkBr3 cells incubated with (A) Cys-NPs (22 μg/mL) and (B) 11A4-NPs (22 μg/mL) at different time points (nuclei are stained in blue, NPs are observed in orange, and the phase contrast image is in gray). The NPs remained in contact with the cells throughout the whole assay (no washing steps). (C) Mean fluorescence intensity in cytoplasm of SkBr3 and MDA-MB-231 cells after incubation with Cys-NPs and 11A4-NPs, data represent mean ± SD (n = 15 imaging fields). Confocal images of SkBr3 cells (D) preincubated for 30 min with free 11A4 (12 μg/mL) followed by incubation for 30 min with 11A4-NPs (80 μg/mL) and (E) incubated for 30 min with 11A4-NPs alone (80 μg/mL). Nuclei are stained in blue, NPs are observed in orange, and the overlay of phase contrast image shows the cell borders. (F) Mean fluorescence intensity in cytoplasm of SkBr3 cells exposed to the competition conditions; data represent mean ± SD (n = 15 imaging fields).

potential suggests that negative amino acid residues are exposed to the medium. In a previous study conducted by our research group, PLGA NPs conjugated to 11A4 also showed a more negative zeta potential than nonconjugated NPs.[66]

In addition to the physicochemical characteristics of the NPs, the efficiency of the conjugation reaction was also determined. Cysteine was conjugated to the NPs with an efficiency of ∼60%. In a previous study, our group reported a similar conjugation efficiency for another small molecule, i.e., cRGDfK, to polymeric NPs via maleimide−thiol chemistry.[66] Theoretically, a 100% conjugation efficiency could have been achieved because a molar excess of cysteine to maleimide (2:1) was used. However, due to the miscibility of PEG and PLGA, it is likely that not all maleimide groups are exposed on the surface of the NPs and available for reaction.[76,77]

The conjugation efficiency of cysteine was similar for placebo and saporin-loaded NPs (formulations 2 and 5). In contrast, the conjugation efficiency of 11A4 was higher for placebo NPs (formulation 3) than for saporin-loaded NPs (formulation 6). As previously mentioned, some saporin molecules can be associated with the surface of the NPs resulting in partial obstruction of nearby maleimide groups and limiting the extent of functionalization of the surface with the nanobody. This steric hindrance may have been less relevant for conjugation to cysteine due to the smaller size of this ligand.

The encapsulation efficiency of saporin in the NPs was 26 ± 2% (n = 2), which corresponded to 0.52 ± 0.03 loading weight % (or 5.2 ± 0.3 μg of saporin/mg NPs). After resuspension in PBS, the NPs showed a very small burst release (<5% of the total saporin content), followed by a sustained release of the protein. An estimation from SDS-PAGE analysis indicates that around 13% of the saporin loading was released from the NPs during 2 days of incubation in PBS (Figure S4). Similar sustained release patterns (10−40% release of protein after 5 days of incubation) have been reported in the literature for protein-loaded PLGA[78,79] and PLGHMGA NPs.[61]

3.3. Cellular Uptake of Targeted and Nontargeted NPs. The kinetics of cellular uptake of Cys-NPs and 11A4-NPs were studied by live confocal microscopy from 15 min to 8 h in SkBr3 (HER2 positive) and MDA-MB-231 (HER2 negative) cells. The binding and uptake of Cys-NPs was poor at all the time points evaluated, as shown by the low fluorescent signal in the cytoplasm of the cells (Figure 2A,C). In contrast, the uptake of 11A4-NPs by SkBr3 cells was already detected at early time points of the study (≤30 min), and it increased over time (Figure 2B,C). Throughout the study, the number of fluorescent

DOI: 10.1021/acs.molpharmaceut.8b01318
Mol. Pharmaceutics 2019, 16, 1633−1647

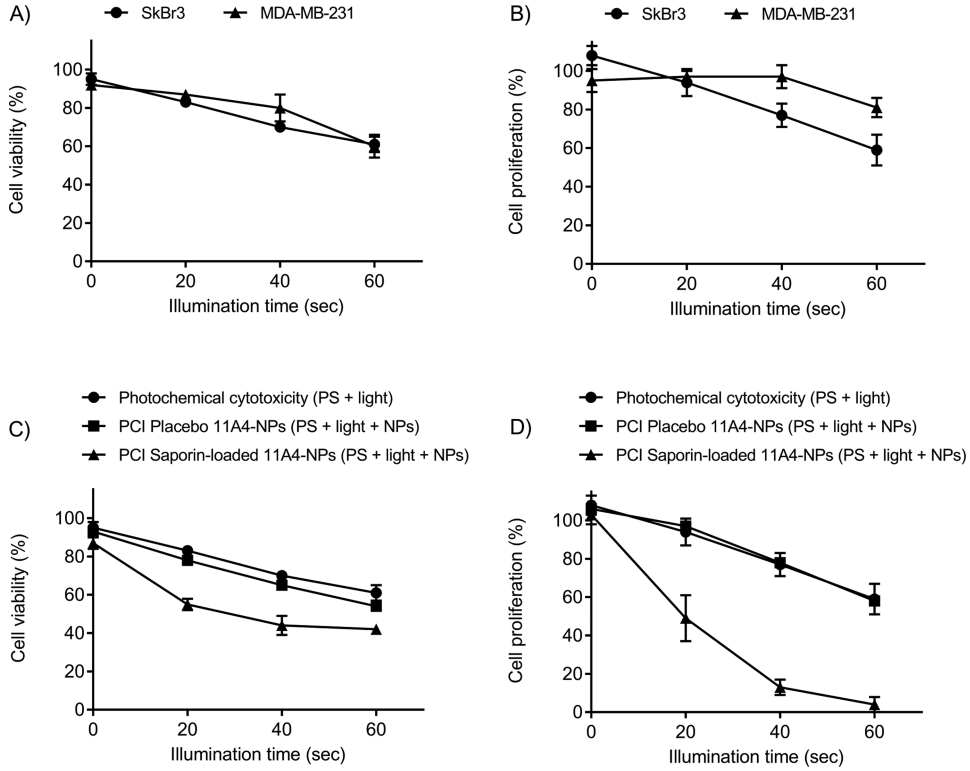

Figure 3. Cytotoxicity of $TPPS_{2a}$ (0.5 μg/mL) combined with different illumination times. (A) Cell viability and (B) cell proliferation of SkBr3 and MDA-MB-231 cells exposed to PS and illumination, without NPs, relative to the nontreated control (no PS, no light). Data represent mean ± SD (n = 6). (C) Cell viability and (D) cell proliferation of SkBr3 cells in the absence and presence of placebo 11A4-NPs and saporin-loaded 11A4-NPs relative to the nontreated control (no PS, no light, no NPs). Final NPs concentration in the wells was 90 μg/mL. Data represent mean ± SD (n = 6 for tests in the absence of NPs, n = 3 tests in the presence of NPs). Illumination for 20, 40, and 60 s corresponds to light doses of ~0.3, 0.5, and 0.8 J/cm^2.

spots per area of cytoplasm was between 8 and 18 times higher in the cells exposed to 11A4-NPs compared to those incubated with Cys-NPs (Figure S5), which indicates an enhanced internalization of 11A4-NPs, likely mediated by the interaction between the nanobody 11A4 and the HER2 receptor. This observation is further supported by the almost negligible uptake of both, 11A4-NPs and Cys-NPs, by the HER2 negative MDA-MB-231 cell line (Figures 2C and S6).

To confirm that the specific uptake of 11A4-NPs was mediated by the interaction of the 11A4 nanobody with the HER2 receptor, competition studies were carried out by preincubating the cells with free 11A4 prior to exposure to 11A4-NPs. Microscopic observations showed that, in the presence of free nanobody, the internalization of 11A4-NPs was considerably inhibited (Figure 2D), as compared to cells incubated with 11A4-NPs in the absence of free nanobody (Figure 2E). Image analysis confirmed that the fluorescent signal of 11A4-NPs inside the cells was remarkably lower in the samples subjected to competition (Figure 2F), thus corroborating the results from the visual observations.

Altogether, the results from the confocal microscopy studies demonstrate that the endocytosis of 11A4-NPs is mediated by the specific interaction between the nanobody 11A4 and the HER2 receptor. Since the focus of the present work is to target HER2 for the treatment of breast cancer, the selective accumulation of the 11A4-NPs was evaluated in HER2 positive cancer cells (SkBr3), using HER2 negative cancer cells (MDA-MB-231) as a negative control. Alternatively, normal cells could also be used as a control since they express 100-fold less HER2 than HER2 positive cancer cells.[80] In that case, it would be expected that the 11A4-NPs would interact similarly with normal cells as with the HER2 negative breast cancer cells (i.e., poor internalization). In addition to our results, other studies from our research group have confirmed that the uptake of nanobody-targeted nanocarriers is truly mediated by specific ligand−receptor interactions. In that regard, the use of a nontumor specific nanobody as ligand resulted in neither binding nor uptake of different types of nanocarriers.[43,47]

In general, the cargo internalized by receptor-mediated endocytosis is initially localized in early endosomes and then sorted to one of several pathways, including the recycling and degradative pathways.[81−83] The uptake images (Figure 2B, at 8 h) suggest that the 11A4-NPs are entrapped in intracellular vesicles, likely late endosomes and/or lysosomes, as proposed by the highly punctuated fluorescence pattern observed in the cytoplasm of SkBr3 cells.[84,85] To prevent that the 11A4-NPs and/or their released cargo (saporin) are degraded in the lysosomes, an external stimulus was applied to induce endosomal escape and to maximize the cytotoxicity of the formulation: i.e., photochemical internalization or PCI.

3.4. Optimization of Photochemical Internalization (PCI). The outcome of PCI is influenced by the concentration of PS and the illumination time.[54,86] In general, high concentrations of PS and long illumination times can induce cell death, here described as photochemical cytotoxicity. In the present work, a concentration of 0.5 μg/mL of PS was chosen based on previous studies conducted in our research group.[54,67] Since the aim was to specifically evaluate the PCI-mediated cytotoxicity of saporin-loaded NPs, it was important to distinguish between the effects of PCI (PS + light + NPs) and the photochemical

DOI: 10.1021/acs.molpharmaceut.8b01318
Mol. Pharmaceutics 2019, 16, 1633−1647

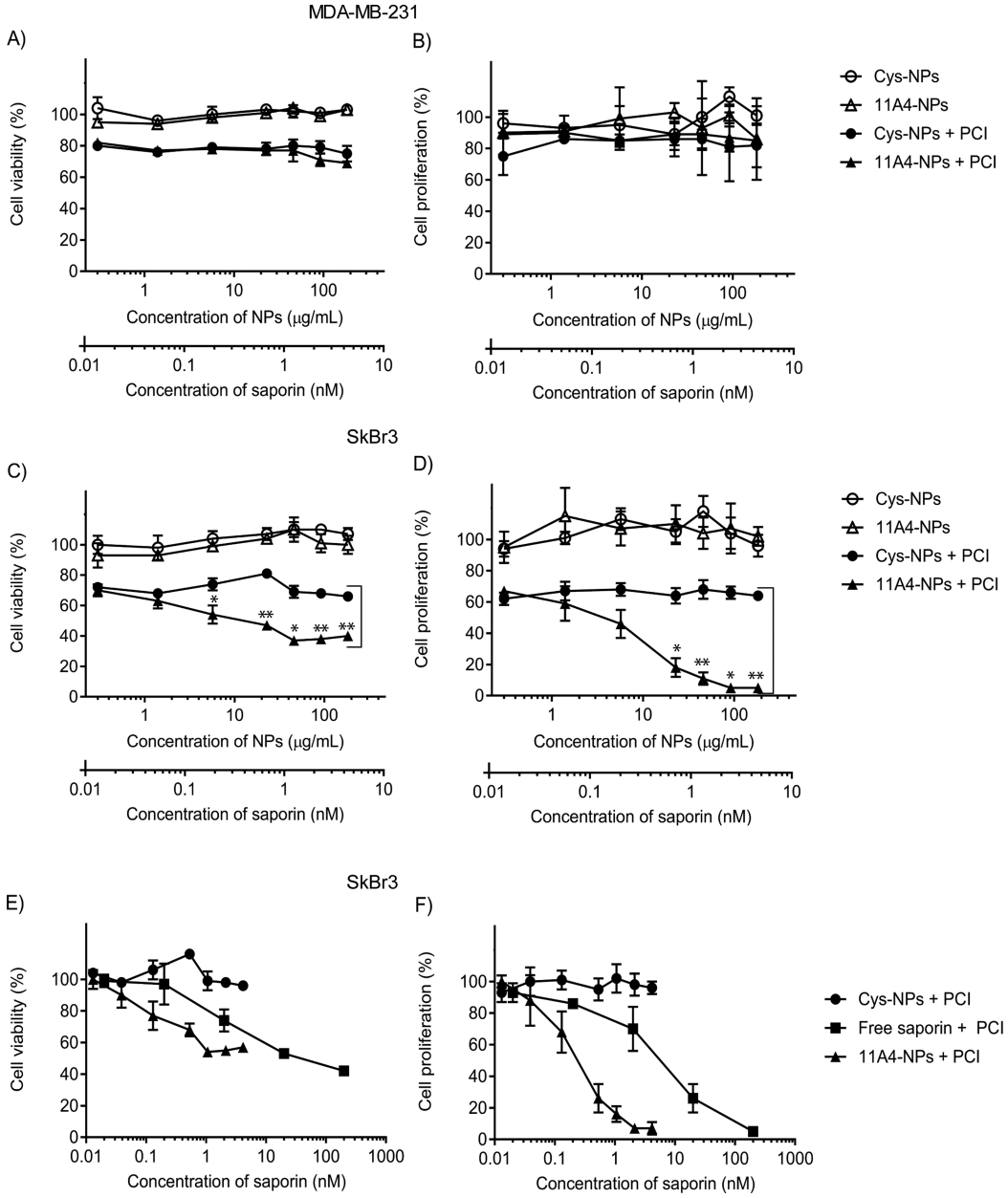

Figure 4. Cytotoxicity of saporin-loaded NPs with or without PCI. The concentration of saporin reported in the graphs is 13% of the dose loaded in the NPs. Cytotoxicity of saporin-loaded NPs on (A,B) MDA-MB-231 and (C,D) SkBr3 cells. Cell viability and cell proliferation were calculated respective to the nontreated control (no PCI, no NPs). (E) Cell viability and (F) cell proliferation of SkBr3 cells incubated with free saporin and saporin-loaded NPs calculated respective to a control exposed to PCI in absence of protein and NPs. This control had 73 ± 5% cell viability and 73 ± 8% cell proliferation relative to a nontreated sample (no PCI, no free protein, no NPs). Data represent mean ± SD ($n = 3$). Data Cys-NPs + PCI vs 11A4-NPs + PCI analyzed by unequal variances t test; *p-value < 0.05 and **p-value < 0.001.

cytotoxicity (PS + light). The illumination time was optimized in a way that PCI was achieved without significantly compromising the viability of cells. To this end, the cytotoxicity of the PS $TPPS_{2a}$ combined with different illumination times was first evaluated on SkBr3 and MDA-MB-231 cells without NPs. For both cell lines, a decrease in cell viability was observed with increasing illumination time up to 60 s (Figure 3A,B). In that time frame, the cell viability decreased by 40% for both SkBr3 and MDA-MB-231, while cellular proliferation decreased by 40% for SkBr3 and by 20% for the MDA-MB-231 cells.

Subsequently, the influence of the different illumination times was studied in combination with the saporin-loaded NPs. At all the illumination times tested, higher cytotoxicity was observed on SkBr3 cells that were incubated with saporin-loaded 11A4-NPs, compared to cells incubated with placebo 11A4-NPs (Figure 3C,D), implying that PCI successfully mediates the endosomal escape of the NPs leading to saporin release in the cytosol. Since 40 s of illumination provided the best compromise between relatively low photochemical cytotoxicity (caused by PS + light) and high cytotoxicity caused by the presence of the saporin-loaded NPs, this setting was chosen for further in depth studies.

3.5. Cytotoxicity of Saporin-loaded Targeted and Untargeted NPs in Combination with PCI. The cytotoxic effect of saporin-loaded Cys-NPs and 11A4-NPs was evaluated in SkBr3 and MDA-MB-231 cells with or without PCI. In

DOI: 10.1021/acs.molpharmaceut.8b01318
Mol. Pharmaceutics 2019, 16, 1633−1647

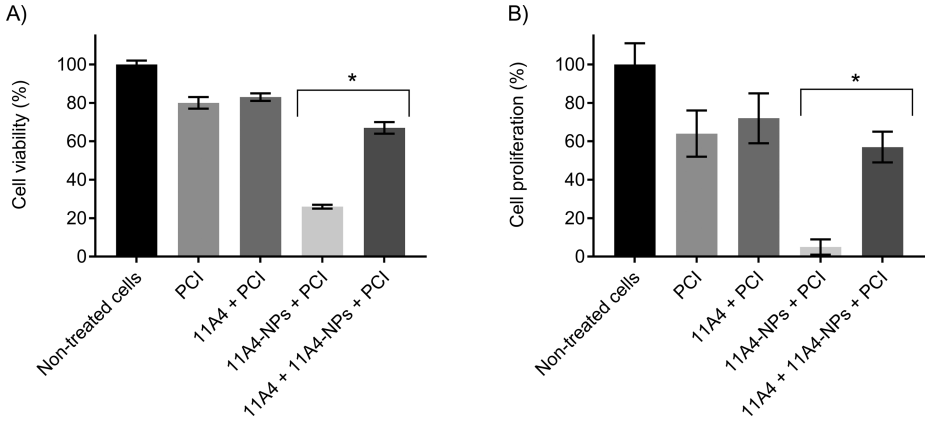

Figure 5. Cytotoxicity of saporin-loaded 11A4-NPs with PCI on SkBr3 cells with and without preincubation with free 11A4. (A) Cell viability and (B) cell proliferation were assessed in cells incubated with 11A4-NPs and subjected to PCI treatment or in cells preincubated with an excess of free 11A4 followed by the addition of 11A4-NPs and PCI treatment. Data represent mean ± SD (n = 3). Data 11A4-NPs + PCI vs 11A4 + 11A4-NPs + PCI analyzed by unequal variances t test; *p-value < 0.05.

parallel, placebo NPs were also investigated, as well as the effect of free saporin. As a control, cells incubated only with PS and with light exposure (no NPs) were compared to nontreated cells (no PS, no light, no NPs).

Placebo Cys-NPs and placebo 11A4-NPs used without PCI neither affected cell viability nor proliferation of SkBr3 (Figure S7A,B) as well as of MDA-MB-231 (Figure S7C,D) cells. Even though a decrease in cell viability and proliferation was observed for both cell lines treated with NPs and PCI, this effect was not dependent on the dose of NPs and can be explained as toxicity induced by the PS applied in combination with light, i.e., photochemical cytotoxicity: compared to a nontreated control, cell viability was 66 ± 3% for SkBr3 and 75 ± 3% for MDA-MB-231, and cell proliferation was 66 ± 3% for SkBr3 and 88 ± 5% for MDA-MB-231. Saporin-loaded Cys- and 11A4-NPs without PCI did not affect the cell viability or proliferation of MDA-MB-231 cells, while incubation of NPs combined with PCI slightly decreased these parameters (Figure 4A,B), which corresponds to the photochemical cytotoxicity: compared to nontreated cells, cell viability was 77 ± 9% and cell proliferation was 91 ± 10%. In addition, the lack of toxicity of both Cys-NPs and 11A4-NPs in MDA-MB-231 cells is in line with the low uptake of these formulations (Figure 2C). Similarly to the results in MDA-MB-231, saporin-loaded Cys- or 11A4-NPs without PCI were not cytotoxic to SkBr3 cells. Incubation of SkBr3 cells with Cys-NPs and PCI slightly and stably decreased cell viability and proliferation, which is in the range of photochemical cytotoxicity reported above: compared to a nontreated control, cell viability was 69 ± 5% and cell proliferation was 67 ± 10%. In contrast, only the incubation of SkBr3 cells with saporin-loaded 11A4-NPs and PCI resulted in a dose-dependent decrease in cell viability and cell proliferation (Figure 4C,D), confirming that the NPs and their content were initially entrapped in the endosome and were subsequently released into the cytosol upon PCI.

At the highest concentrations tested, the saporin-loaded 11A4-NPs combined with PCI reduced the cell proliferation of SkBr3 cells by ∼95% and the cell viability by ∼60%. The residual metabolic activity of the cells detected in the viability studies could be explained by the ability of saporin to induce apoptosis which, being energy-dependent, requires the cells to remain active in order to provide energy until late stages of the process.[87] Taken together, the results of Figure 4C,D demonstrate that, when loaded in NPs, effective saporin delivery is fully dependent on HER2 targeting and PCI, which is favorable for enhancing the selectivity of the therapy. Other studies have shown that PCI enhances the efficacy of untargeted nanocarriers, loaded with or conjugated to cytotoxic agents,[88−91] although in these cases the selectivity of these nanocarriers toward specific cells was not evaluated.

The dose-dependent cytotoxicity of free saporin (i.e., not encapsulated in the NPs) was compared to the cytotoxicity induced by saporin-loaded NPs on SkBr3 cells when used in combination with PCI (Figure 4E,F). In this particular study, the dose of free saporin added to the cells is compared to the concentration of saporin expected to be released from the NPs after 2 days of incubation with the cells based on the release studies conducted in PBS (13% release, Figure S4). Nevertheless, it is possible that more saporin was released from the NPs in cell culture medium/intracellularly, compared to PBS, as shown for other compounds.[92] Based on the cell proliferation assays (Figure 4F), the EC_{50} of saporin when delivered by 11A4-NPs and PCI, estimated at 0.3 nM (n = 6, 95% CI = 0.25−0.34) was substantially lower (15-fold difference) than the EC_{50} for free saporin administered in combination with PCI, i.e., 4.5 nM (n = 6, 95% CI = 3.5−5.7). In addition, the dose−response profiles of saporin-loaded Cys- and 11A4-NPs differ significantly, indicating that the cytotoxicity from saporin-loaded 11A4-NPs is most likely caused by the intracellular release of saporin after the internalization of these HER2 targeted NPs, and not by PCI of free saporin.

Interestingly, saporin in its free form was not toxic to the cells here investigated when administered without PCI (Figure S8A−D). In contrast, combination of free saporin with PCI exhibited cytotoxic effect on both cell lines, although the effect was lower in MDA-MB-231 (EC_{50} = 67 nM, n = 6, 95% CI = 43−111) than in SkBr3 (EC_{50} = 4.5 nM, n = 6, 95% CI = 3.5−5.7). Cell line-dependent differences of the effects of saporin have also been reported in other studies.[9,93] Remarkably, saporin-induced cytotoxicity has also been reported even when it is administered without PCI or any other endosomal escape technique.[4,71,94] Therefore, administration of free saporin *in vivo* could result in substantial toxicity in nontargeted cells and tissues. This problem can be overcome by encapsulating saporin in receptor-targeted nanoparticles, which combined with PCI, can lead to selective and local delivery to the cytosol of the

DOI: 10.1021/acs.molpharmaceut.8b01318
Mol. Pharmaceutics 2019, 16, 1633−1647

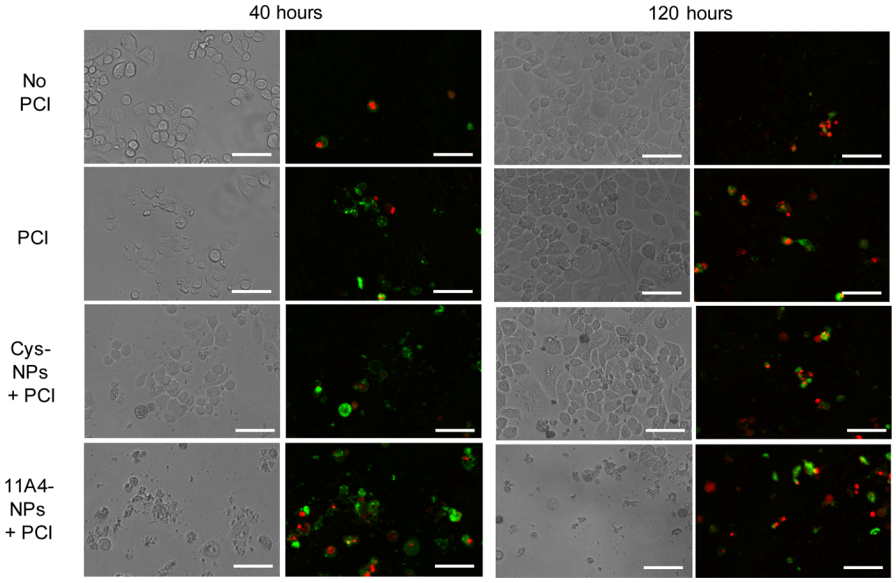

Figure 6. Microscopic observations of SkBr3 cells at 40 and 120 h after treatment with saporin-loaded NPs and/or PCI. Representative images obtained by phase contrast and by overlay of the channels depicting the signals for Annexin V-FITC (apoptotic cells, in green) and PI (dead cells, in red). Scale bar = 100 μm.

targeted cells, as proposed by the *in vitro* data presented in this work. While the *in vivo* evaluation of the efficacy of saporin-loaded 11A4-NPs combined with PCI is beyond the scope of the present Article, some considerations for the *in vivo* translation of this treatment include (1) reducing the size of the NPs for more efficient extravasation and passive accumulation in the tumor site (favorable for nanocarriers with sizes <200 nm[95,96]) and (2) using photosensitizers such as $TPCS_{2a}$,[97] which are activated at wavelengths that are optimal for tissue penetration, i.e., 600–800 nm. Furthermore, the treatment proposed in this Article should be envisioned for use in combination with other cancer therapies in order to efficiently treat heterogeneous tumors in which only some cells express the HER2 receptor, and to decrease the chances for development of cancer drug resistance.

To further investigate the selectivity of the cytotoxicity of the 11A4-NPs, competition assays were performed. When the cells were preincubated with free 11A4, subsequent incubation with 11A4-NPs and PCI application did not substantially decrease cell proliferation or cell viability, in contrast with cells that were not preincubated with the free nanobody (Figure 5). These results are in agreement with confocal microscopy observations, where preincubation with free 11A4 inhibited the cellular uptake of 11A4-NPs (Figure 2D,F).

Similar to our findings, a previous study on the effect of saporin-loaded EGFR-targeted liposomes on OVCAR-3 cells also highlighted the advantages of combining the use of targeted nanocarriers with PCI.[54] While high uptake and cytotoxicity were observed for the EGFR-targeted liposomes, the non-targeted liposomes were also internalized and cytotoxic, though to a lesser extent. In contrast, the nontargeted NPs used in our work did not show any uptake or cytotoxicity, indicating that our system has improved selectivity over the aforementioned liposomes. Targeting, as achieved by the 11A4-NPs, can induce clustering of HER2 and promote its internalization,[98−100] resulting in efficient receptor-mediated endocytosis of the NPs and subsequent intracellular delivery of its cytotoxic cargo (saporin).

Other types of nanocarriers, such as nanogels and lipopepsomes, have also been successfully used for the targeted intracellular delivery of saporin in cancer cells. These nanocarriers were not used in combination with PCI, instead they achieved endosomal escape by membrane destabilization[16] or by membrane fusion driven by coiled-coil motifs.[19] Although direct comparison between these studies is difficult due to the different nature of the nanocarriers and targeted cell lines, these studies suggest other approaches are also effective in ensuring endosomal escape of saporin.

3.6. Cell Death Mechanism Induced by Saporin-loaded 11A4-NPs and PCI. Microscopic observations of cells treated with saporin-loaded 11A4-NPs and PCI, 40 and 120 h after illumination, revealed significant morphological alterations suggesting apoptosis (Figure 6). In contrast, only a few cells with morphological alterations were observed in the cells subjected to PCI only or to Cys-NPs and PCI. A striking difference in the cell number was also observed, particularly at the 120 h time point: while there are only a few cells left after treatment with 11A4-NPs and PCI, a large number of cells are present in the samples exposed to PCI only (i.e., photochemical cytotoxicity). These observations are in agreement with the results from the cytotoxicity assays (Figure 4), which indicated that the decrease in cell viability caused by saporin-loaded 11A4-NPs combined with PCI is accompanied by a strong antiproliferative effect.

The visual analysis of cells exposed to PCI (with or without incubation with NPs) and stained with Annexin V/PI revealed a fluorescent pattern indicative of apoptosis both in its early and late stages, though the intensity of the fluorescent signal (and extent of apoptosis) differed between samples (Figure 6; noncropped images, Figure S9A). In contrast, a very low fluorescent signal was observed for cells not exposed to PCI (even when incubated with NPs). The highest Annexin V signal was observed for the cells incubated with saporin-loaded 11A4-NPs combined with PCI 40 h after illumination (Figure S9B). While in this sample the signal is more intense for Annexin V than for PI at the 40 h time point, both signals have similar intensities at the 120 h time point (Figure 6), indicating an increase in the number of cells undergoing late apoptosis/secondary necrosis at that time. This implies an efficient but

DOI: 10.1021/acs.molpharmaceut.8b01318
Mol. Pharmaceutics 2019, 16, 1633−1647

relatively slow onset and progression of apoptosis. While apoptosis is often depicted as an event that lasts between 12 and 24 h,[101] longer times could be required for cell death due to the asynchronous nature of the process and to its susceptibility to factors such as cell type and the nature and intensity of the apoptotic stimulus.

4. CONCLUSION

The findings presented in this Article show that saporin-loaded PEG−PLGHMGA NPs decorated with the 11A4 nanobody in combination with PCI can be used to selectively induce cell death of HER2 positive breast cancer cells. The selectivity of this system is a consequence of the specific interactions between the 11A4 nanobodies on the NPs and the HER2 receptors on the cell surface, which result in receptor-mediated endocytosis of the NPs. Precise light exposure during the subsequent PCI allows for the time- and space-controlled release of the NPs and/or their cargo from the endosome, thereby exposing the cells to the cytotoxic effects of saporin. The tailorability of PEG−PLGHMGA NPs is an added advantage to the system under study, for instance, the NPs could be loaded with proteins other than saporin. In conclusion, the tailorability, selectivity, and efficiency of the 11A4-NPs used in combination with PCI makes them a promising modality for cancer treatment.

■ ASSOCIATED CONTENT

Supporting Information

The Supporting Information is available free of charge on the ACS Publications website at DOI: 10.1021/acs.molpharmaceut.8b01318.

> DSC thermograms of PLGHMGA and $MePEG_{2000}$−PLGHMGA, ^{1}H NMR spectra of PLGHMGA and MePEG−PLGHMGA, superimposed ^{1}H NMR spectra of PLGBMGA and PLGHMGA, SDS-PAGE gel of the saporin *in vitro* release study, additional information on uptake of targeted and nontargeted NPs by SkBr3 cells, cytotoxicity of placebo NPs with or without PCI, cytotoxicity of free saporin with or without PCI, and noncropped images of microscopic observations of SkBr3 cells stained with Annexin V−FITC/PI (PDF)

■ AUTHOR INFORMATION

Corresponding Author

*E-mail: S.Oliveira@uu.nl. Phone: +31 63 410 3460. Fax: +31 30 251 7839.

ORCID

Cornelus F. van Nostrum: 0000-0003-4210-5241

Wim E. Hennink: 0000-0002-5750-714X

Sabrina Oliveira: 0000-0002-6011-2122

Notes

The authors declare no competing financial interest.

■ ACKNOWLEDGMENTS

The authors would like to thank Dr. Anders Høgset for providing the photosensitizer $TPPS_{2a}$ used in this study and MSc Irati Beltrán Hernández for her guidance in the apoptosis assays. Lucía Martínez-Jothar would like to thank the Consejo Nacional de Ciencia y Tecnología (CONACyT), México (grant no. 384743) for the funding provided in the framework of her Ph.D.

■ REFERENCES

(1) Nurgali, K.; Jagoe, R. T.; Abalo, R. Editorial: Adverse effects of cancer chemotherapy: Anything new to improve tolerance and reduce sequelae? *Front. Pharmacol.* **2018**, *9*, 1−3.

(2) Santanché, S.; Bellelli, A.; Brunori, M. The unusual stability of saporin, a candidate for the synthesis of immunotoxins. *Biochem. Biophys. Res. Commun.* **1997**, *234*, 129−132.

(3) Polito, L.; Bortolotti, M.; Mercatelli, D.; Battelli, M. G.; Bolognesi, A. Saporin-S6: A useful tool in cancer therapy. *Toxins* **2013**, *5*, 1698−1722.

(4) Bagga, S.; Seth, D.; Batra, J. K. The cytotoxic activity of ribosome-inactivating protein saporin-6 is attributed to its rRNA N-glycosidase and internucleosomal DNA fragmentation activities. *J. Biol. Chem.* **2003**, *278*, 4813−4820.

(5) Sikriwal, D.; Ghosh, P.; Batra, J. K. Ribosome inactivating protein saporin induces apoptosis through mitochondrial cascade, independent of translation inhibition. *Int. J. Biochem. Cell Biol.* **2008**, *40*, 2880−2888.

(6) Polito, L.; Bortolotti, M.; Farini, V.; Battelli, M. G.; Barbieri, L.; Bolognesi, A. Saporin induces multiple death pathways in lymphoma cells with different intensity and timing as compared to ricin. *Int. J. Biochem. Cell Biol.* **2009**, *41*, 1055−1061.

(7) Cimini, A.; Mei, S.; Benedetti, E.; Laurenti, G.; Koutris, I.; Cinque, B.; Cifone, M. G.; Galzio, R.; Pitari, G.; Di Leandro, L.; Giansanti, F.; Lombardi, A.; Fabbrini, M. S.; Ippoliti, R. Distinct cellular responses induced by saporin and a transferrin-saporin conjugate in two different human glioblastoma cell lines. *J. Cell. Physiol.* **2012**, *227*, 939−951.

(8) Cavallaro, U.; Nykjaer, A.; Nielsen, M.; Soria, M. R. α2-macroglobulin receptor mediates binding and cytotoxicity of plant ribosome-inactivating proteins. *Eur. J. Biochem.* **1995**, *232*, 165−171.

(9) Ferreras, J.; Barbieri, L.; Girbés, T.; Battelli, M. G.; Rojo, M. A.; Arias, F. J.; Rocher, M. A.; Soriano, F.; Mendéz, E.; Stirpe, F. Distribution and properties of major ribosome-inactivating proteins (28 S rRNA N-glycosidases) of the plant Saponaria officinalis L. (Caryophyllaceae). *Biochim. Biophys. Acta, Gene Struct. Expression* **1993**, *1216*, 31−42.

(10) Polito, L.; Bortolotti, M.; Pedrazzi, M.; Bolognesi, A. Immunotoxins and other conjugates containing saporin-s6 for cancer therapy. *Toxins* **2011**, *3*, 697−720.

(11) Gilabert-Oriol, R.; Thakur, M.; Von Mallinckrodt, B.; Hug, T.; Wiesner, B.; Eichhorst, J.; Melzig, M. F.; Fuchs, H.; Weng, A. Modified trastuzumab and cetuximab mediate efficient toxin delivery while retaining antibody-dependent cell-mediated cytotoxicity in target cells. *Mol. Pharmaceutics* **2013**, *10*, 4347−4357.

(12) Gilabert-oriol, R.; Weng, A.; Mallinckrodt, B. V.; Melzig, M. F.; Fuchs, H. Immunotoxins constructed with ribosome-inactivating proteins and their enhancers: A lethal cocktail with tumor specific efficacy proteins. *Curr. Pharm. Des.* **2014**, *20*, 6584−6643.

(13) Giansanti, F.; Flavell, D. J.; Angelucci, F.; Fabbrini, M. S.; Ippoliti, R. Strategies to improve the clinical utility of saporin-based targeted toxins. *Toxins* **2018**, *10*, 1−32.

(14) Alewine, C.; Hassan, R.; Pastan, I. Advances in anticancer immunotoxin therapy. *Oncologist* **2015**, *20*, 176−185.

(15) Li, M.; Liu, Z. S.; Liu, X. L.; Hui, Q.; Lu, S. Y.; Qu, L. L.; Li, Y. S.; Zhou, Y.; Ren, H. L.; Hu, P. Clinical targeting recombinant immunotoxins for cancer therapy. *OncoTargets Ther.* **2017**, *10*, 3645−3665.

(16) Qiu, M.; Zhang, Z.; Wei, Y.; Sun, H.; Meng, F.; Deng, C.; Zhong, Z. Small-Sized and Robust Chimaeric Lipopepsomes: A Simple and Functional Platform with High Protein Loading for Targeted Intracellular Delivery of Protein Toxin in Vivo. *Chem. Mater.* **2018**, *30*, 6831−6838.

(17) Jiang, Y.; Yang, W.; Zhang, J.; Meng, F.; Zhong, Z. Protein Toxin Chaperoned by LRP-1-Targeted Virus-Mimicking Vesicles Induces High-Efficiency Glioblastoma Therapy In Vivo. *Adv. Mater.* **2018**, *30*, 1−7.

(18) Jiang, Y.; Zhang, J.; Meng, F.; Zhong, Z. Apolipoprotein e Peptide-Directed Chimeric Polymersomes Mediate an Ultrahigh-Efficiency Targeted Protein Therapy for Glioblastoma. *ACS Nano* **2018**, *12*, 11070−11079.

(19) Ding, L.; Jiang, Y.; Zhang, J.; Klok, H. A.; Zhong, Z. pH-Sensitive Coiled-Coil Peptide-Cross-Linked Hyaluronic Acid Nanogels: Synthesis and Targeted Intracellular Protein Delivery to CD44 Positive Cancer Cells. *Biomacromolecules* **2018**, *19*, 555−562.
(20) Lächelt, U.; Wagner, E. Nucleic acid therapeutics using polyplexes: A journey of 50 years (and beyond). *Chem. Rev.* **2015**, *115*, 11043−11078.
(21) Li, D.; van Nostrum, C. F.; Mastrobattista, E.; Vermonden, T.; Hennink, W. E. Nanogels for intracellular delivery of biotherapeutics. *J. Controlled Release* **2017**, *259*, 16−28.
(22) Cheng, L.; Yang, L.; Meng, F.; Zhong, Z. Protein Nanotherapeutics as an Emerging Modality for Cancer Therapy. *Adv. Healthcare Mater.* **2018**, *7*, 1−9.
(23) Onoue, S.; Yamada, S.; Chan, H. K. Nanodrugs: Pharmacokinetics and safety. *Int. J. Nanomed.* **2014**, *9*, 1025−1037.
(24) Pérez-Herrero, E.; Fernández-Medarde, A. Advanced targeted therapies in cancer: Drug nanocarriers, the future of chemotherapy. *Eur. J. Pharm. Biopharm.* **2015**, *93*, 52−79.
(25) Leemhuis, M.; Kruijtzer, J. A. W.; van Nostrum, C. F.; Hennick, W. E. In vitro hydrolytic degradation of hydroxyl-functionalized poly(α-hydroxy acid)s. *Biomacromolecules* **2007**, *8*, 2943−2949.
(26) Shirangi, M.; Hennink, W. E.; Somsen, G. W.; Van Nostrum, C. F. Identification and assessment of octreotide acylation in polyester microspheres by LC-MS/MS. *Pharm. Res.* **2015**, *32*, 3044−3054.
(27) Ghassemi, A. H.; van Steenbergen, M. J.; Barendregt, A.; Talsma, H.; Kok, R. J.; van Nostrum, C. F.; Crommelin, D. J. A.; Hennink, W. E. Controlled Release of Octreotide and Assessment of Peptide Acylation from Poly(D,L-lactide-co-hydroxymethyl glycolide) Compared to PLGA Microspheres. *Pharm. Res.* **2012**, *29* (1), 110−120.
(28) van der Meel, R.; Vehmeijer, L. J. C.; Kok, R. J.; Storm, G.; van Gaal, E. V. B. Ligand-targeted particulate nanomedicines undergoing clinical evaluation: Current status. *Adv. Drug Delivery Rev.* **2013**, *65*, 1284−1298.
(29) Zhong, Y.; Meng, F.; Deng, C.; Zhong, Z. Ligand-directed active tumor-targeting polymeric nanoparticles for cancer chemotherapy. *Biomacromolecules* **2014**, *15*, 1955−1969.
(30) Prabhu, R. H.; Patravale, V. B.; Joshi, M. D. Polymeric nanoparticles for targeted treatment in oncology: Current insights. *Int. J. Nanomed.* **2015**, *10*, 1001−1018.
(31) Serna, N.; Sánchez-García, L.; Unzueta, U.; Díaz, R.; Vázquez, E.; Mangues, R.; Villaverde, A. Protein-based therapeutic killing for cancer therapies. *Trends Biotechnol.* **2018**, *36* (3), 318−335.
(32) Muyldermans, S.; Lauwereys, M. Unique single-domain antigen binding fragments derived from naturally occurring camel heavy-chain antibodies. *J. Mol. Recognit.* **1999**, *12*, 131−140.
(33) Kolkman, J. A.; Law, D. A. Nanobodies - from llamas to therapeutic proteins. *Drug Discovery Today: Technol.* **2010**, *7* (2), e139−e146.
(34) Oliveira, S.; Heukers, R.; Sornkom, J.; Kok, R. J.; Van Bergen En Henegouwen, P. M. P. Targeting tumors with nanobodies for cancer imaging and therapy. *J. Controlled Release* **2013**, *172*, 607−617.
(35) Arbabi-Ghahroudi, M. Camelid single-domain antibodies: Historical perspective and future outlook. *Front. Immunol.* **2017**, *8*, 1−8.
(36) Vincke, C.; Loris, R.; Saerens, D.; Martinez-Rodriguez, S.; Muyldermans, S.; Conrath, K. General strategy to humanize a camelid single-domain antibody and identification of a universal humanized nanobody scaffold. *J. Biol. Chem.* **2009**, *284*, 3273−3284.
(37) Tai, W.; Mahato, R.; Cheng, K. The role of HER2 in cancer therapy and targeted drug delivery. *J. Controlled Release* **2010**, *146*, 264−275.
(38) Omar, N.; Yan, B.; Salto-Tellez, M. HER2: An emerging biomarker in non-breast and non-gastric cancers. *Pathogenesis* **2015**, *2*, 1−9.
(39) Kijanka, M.; Warnders, F.-J.; El Khattabi, M.; Lub-de Hooge, M.; van Dam, G. M.; Ntziachristos, V.; de Vries, L.; Oliveira, S.; van Bergen en Henegouwen, P. M. P. Rapid optical imaging of human breast tumour xenografts using anti-HER2 VHHs site-directly conjugated to IRDye 800CW for image-guided surgery. *Eur. J. Nucl. Med. Mol. Imaging* **2013**, *40*, 1718−1729.
(40) Kijanka, M. M.; van Brussel, A. S. A.; van der Wall, E.; Mali, W. P. T. M.; van Diest, P. J.; van Bergen en Henegouwen, P. M. P.; Oliveira, S. Optical imaging of pre-invasive breast cancer with a combination of VHHs targeting CAIX and HER2 increases contrast and facilitates tumour characterization. *EJNMMI Res.* **2016**, *6*, 14.
(41) Kijanka, M.; van Donselaar, E. G.; Müller, W. H.; Dorresteijn, B.; Popov-Celeketic, D.; el Khattabi, M.; Verrips, C. T.; van Bergen en Henegouwen, P. M. P.; Post, J. A. A novel immuno-gold labeling protocol for nanobody-based detection of HER2 in breast cancer cells using immuno-electron microscopy. *J. Struct. Biol.* **2017**, *199*, 1−11.
(42) Oliveira, S.; Schiffelers, R. M.; van der Veeken, J.; van der Meel, R.; Vongpromek, R.; van Bergen en Henegouwen, P. M. P.; Storm, G.; Roovers, R. C. Downregulation of EGFR by a novel multivalent nanobody-liposome platform. *J. Controlled Release* **2010**, *145*, 165−175.
(43) Van Der Meel, R.; Oliveira, S.; Altintas, I.; Haselberg, R.; Van Der Veeken, J.; Roovers, R. C.; Van Bergen En Henegouwen, P. M. P.; Storm, G.; Hennink, W. E.; Schiffelers, R. M.; Kok, R. J. Tumor-targeted nanobullets: Anti-EGFR nanobody-liposomes loaded with anti-IGF-1R kinase inhibitor for cancer treatment. *J. Controlled Release* **2012**, *159*, 281−289.
(44) Talelli, M.; Rijcken, C. J. F.; Oliveira, S.; Van Der Meel, R.; Van Bergen En Henegouwen, P. M. P.; Lammers, T.; Van Nostrum, C. F.; Storm, G.; Hennink, W. E. Nanobody - Shell functionalized thermosensitive core-crosslinked polymeric micelles for active drug targeting. *J. Controlled Release* **2011**, *151*, 183−192.
(45) Talelli, M.; Oliveira, S.; Rijcken, C. J. F.; Pieters, E. H. E.; Etrych, T.; Ulbrich, K.; van Nostrum, R. C. F.; Storm, G.; Hennink, W. E.; Lammers, T. Intrinsically active nanobody-modified polymeric micelles for tumor-targeted combination therapy. *Biomaterials* **2013**, *34*, 1255−1260.
(46) Altintas, I.; Heukers, R.; Van Der Meel, R.; Lacombe, M.; Amidi, M.; Van Bergen En Henegouwen, P. M. P.; Hennink, W. E.; Schiffelers, R. M.; Kok, R. J. Nanobody-albumin nanoparticles (NANAPs) for the delivery of a multikinase inhibitor 17864 to EGFR overexpressing tumor cells. *J. Controlled Release* **2013**, *165*, 110−118.
(47) Heukers, R.; Altintas, I.; Raghoenath, S.; De Zan, E.; Pepermans, R.; Roovers, R. C.; Haselberg, R.; Hennink, W. E.; Schiffelers, R. M.; Kok, R. J.; Van Bergen en Henegouwen, P. M. P. Targeting hepatocyte growth factor receptor (Met) positive tumor cells using internalizing nanobody-decorated albumin nanoparticles. *Biomaterials* **2014**, *35*, 601−610.
(48) Zou, T.; Dembele, F.; Beugnet, A.; Sengmanivong, L.; Trepout, S.; Marco, S.; Marco, A. d.; Li, M. H. Nanobody-functionalized PEG-b-PCL polymersomes and their targeting study. *J. Biotechnol.* **2015**, *214*, 147−155.
(49) Sahay, G.; Alakhova, D. Y.; Kabanov, A. V. Endocytosis of nanomedicines. *J. Controlled Release* **2010**, *145*, 182−195.
(50) Varkouhi, A. K.; Scholte, M.; Storm, G.; Haisma, H. J. Endosomal escape pathways for delivery of biologicals. *J. Controlled Release* **2011**, *151*, 220−228.
(51) Canton, I.; Battaglia, G. Endocytosis at the nanoscale. *Chem. Soc. Rev.* **2012**, *41*, 2718.
(52) Selby, L. I.; Cortez-Jugo, C. M.; Such, G. K.; Johnston, A. P. R. Nanoescapology: progress toward understanding the endosomal escape of polymeric nanoparticles. *Wiley Interdiscip. Rev.: Nanomed. Nanobiotechnol.* **2017**, *9*, e1452.
(53) Selbo, P.; Høgset, A.; Prasmickaite, L.; Berg, K. Photochemical Internalisation: A novel drug delivery system. *Tumor Biol.* **2002**, *23*, 103−112.
(54) Fretz, M. M.; Hogset, A.; Koning, G. A.; Jiskoot, W.; Storm, G. Cytosolic delivery of liposomally targeted proteins induced by photochemical internalization. *Pharm. Res.* **2007**, *24*, 2040−2047.
(55) Selbo, P. K.; Weyergang, A.; Høgset, A.; Norum, O. J.; Berstad, M. B.; Vikdal, M.; Berg, K. Photochemical internalization provides time- and space-controlled endolysosomal escape of therapeutic molecules. *J. Controlled Release* **2010**, *148*, 2−12.

DOI: 10.1021/acs.molpharmaceut.8b01318
Mol. Pharmaceutics 2019, 16, 1633−1647

(56) Bostad, M.; Kausberg, M.; Weyergang, A.; Olsen, C. E.; Berg, K.; Høgset, A.; Selbo, P. K. Light-triggered, efficient cytosolic release of IM7-saporin targeting the putative cancer stem cell marker CD44 by photochemical internalization. *Mol. Pharmaceutics* **2014**, *11*, 2764−2776.
(57) Sultan, A. A.; Jerjes, W.; Berg, K.; Høgset, A.; Mosse, C. A.; Hamoudi, R.; Hamdoon, Z.; Simeon, C.; Carnell, D.; Forster, M.; Hopper, C. Disulfonated tetraphenyl chlorin (TPCS2a)-induced photochemical internalisation of bleomycin in patients with solid malignancies: a phase 1, dose-escalation, first-in-man trial. *Lancet Oncol.* **2016**, *17*, 1217−1229.
(58) Selbo, P. K.; Finnesand, L.; Ekholt, K.; Berg, K.; Høgset, A.; Sturgess, R. Photochemical internalization (PCI) of gemcitabine and chemotherapy for the treatment of cholangiocarcinomas − From lab bench to bedside. *Photodiagn. Photodyn. Ther.* **2017**, *17*, A29.
(59) Leemhuis, M.; van Nostrum, C. F.; Kruijtzer, J. A. W.; Zhong, Z. Y.; ten Breteler, M. R.; Dijkstra, P. J.; Feijen, J.; Hennink, W. E. Functionalized Poly(α-hydroxy acid)s via Ring-Opening Polymerization: Toward Hydrophilic Polyesters with Pendant Hydroxyl Groups. *Macromolecules* **2006**, *39* (10), 3500−3508.
(60) Berg, K.; Western, A.; Bommer, J. C.; Moan, J. Intracellular localization of sulfonated meso-tetraphenylporphines in a human carcinoma cell line. *Photochem. Photobiol.* **1990**, *52* (3), 481−487.
(61) Samadi, N.; van Steenbergen, M. J.; van den Dikkenberg, J. B.; Vermonden, T.; van Nostrum, C. F.; Amidi, M.; Hennink, W. E. Nanoparticles based on a hydrophilic polyester with a sheddable PEG coating for protein delivery. *Pharm. Res.* **2014**, *31*, 2593−2604.
(62) Samadi, N. Biodegradable nanoparticles based on aliphatic polyesters; towards intracellular delivery of protein therapeutics. Ph.D. Thesis, Utrecht University, Utrecht, the Netherlands, 2014.
(63) Péan, J. M.; Venier-Julienne, M. C.; Filmon, R.; Sergent, M.; Phan-Tan-Luu, R.; Benoit, J. P. Optimization of HSA and NGF encapsulation yields in PLGA microparticles. *Int. J. Pharm.* **1998**, *166*, 105−115.
(64) Zambaux, M. F.; Bonneaux, F.; Gref, R.; Maincent, P.; Dellacherie, E.; Alonso, M. J. Influence of experimental parameters on the characteristics of poly (lactic acid) nanoparticles prepared by a double emulsion method. *J. Controlled Release* **1998**, *50*, 31−40.
(65) Sah, H. A new strategy to determine the actual protein content of poly(lactide- co-glycolide) microspheres. *J. Pharm. Sci.* **1997**, *86*, 1315−1318.
(66) Martínez-Jothar, L.; Doulkeridou, S.; Schiffelers, R. M.; Sastre Torano, J.; Oliveira, S.; van Nostrum, C. F.; Hennink, W. E. Insights into maleimide-thiol conjugation chemistry: Conditions for efficient surface functionalization of nanoparticles for receptor targeting. *J. Controlled Release* **2018**, *282*, 101−109.
(67) Oliveira, S.; Fretz, M. M.; Høgset, A.; Storm, G.; Schiffelers, R. M. Photochemical internalization enhances silencing of epidermal growth factor receptor through improved endosomal escape of siRNA. *Biochim. Biophys. Acta, Biomembr.* **2007**, *1768*, 1211−1217.
(68) Weyergang, A.; Selbo, P. K.; Berg, K. Y1068 phosphorylation is the most sensitive target of disulfonated tetraphenylporphyrin-based photodynamic therapy on epidermal growth factor receptor. *Biochem. Pharmacol.* **2007**, *74* (2), 226−35.
(69) Rampersad, S. N. Multiple applications of alamar blue as an indicator of metabolic function and cellular health in cell viability bioassays. *Sensors* **2012**, *12*, 12347−12360.
(70) Gupta, S.; Chan, D. W.; Zaal, K. J.; Kaplan, M. J. A high-throughput real-time imaging technique to quantify netosis and distinguish mechanisms of cell death in human neutrophils. *J. Immunol.* **2018**, *200*, 869−879.
(71) Bagga, S.; Hosur, M. V.; Batra, J. K. Cytotoxicity of ribosome-inactivating protein saporin is not mediated through α2-macroglobulin receptor. *FEBS Lett.* **2003**, *541*, 16−20.
(72) Kichler, A.; Remy, J. S.; Boussif, O.; Frisch, B.; Boeckler, C.; Behr, J. P.; Schuber, F. Efficient gene delivery with neutral complexes of lipospermine and thiol reactive phospholipids. *Biochem. Biophys. Res. Commun.* **1995**, *209*, 444−450.
(73) Li, T.; Takeoka, S. Enhanced cellular uptake of maleimide-modified liposomes via thiol-mediated transport. *Int. J. Nanomed.* **2014**, *9*, 2849−2861.
(74) Jeong, J. H.; Lim, D. W.; Han, D. K.; Park, T. G. Synthesis, characterization and protein adsorption behaviors of PLGA/PEG di-block co-polymer blend films. *Colloids Surf., B* **2000**, *18*, 371−379.
(75) Rafati, A.; Boussahel, A.; Shakesheff, K. M.; Shard, A. G.; Roberts, C. J.; Chen, X.; Scurr, D. J.; Rigby-Singleton, S.; Whiteside, P.; Alexander, M. R.; Davies, M. C. Chemical and spatial analysis of protein loaded PLGA microspheres for drug delivery applications. *J. Controlled Release* **2012**, *162*, 321−329.
(76) Malzert, A.; Boury, F.; Saulnier, P.; Benoit, J. P.; Proust, J. E. Interfacial Properties of Mixed Polyethylene Glycol/Poly(d,l-lactide-co-glycolide) Films Spread at the Air/Water Interface. *Langmuir* **2000**, *16* (4), 1861−1867.
(77) Javiya, C.; Jonnalagadda, S. Physicochemical characterization of spray-dried PLGA/PEG microspheres, and preliminary assessment of biological response. *Drug Dev. Ind. Pharm.* **2016**, *42* (9), 1504−1514.
(78) Samadi, N.; Abbadessa, A.; Di Stefano, A.; Van Nostrum, C. F.; Vermonden, T.; Rahimian, S.; Teunissen, E. A.; Van Steenbergen, M. J.; Amidi, M.; Hennink, W. E. The effect of lauryl capping group on protein release and degradation of poly(d,l-lactic-co-glycolic acid) particles. *J. Controlled Release* **2013**, *172*, 436−443.
(79) Rietscher, R.; Czaplewska, J. A.; Majdanski, T. C.; Gottschaldt, M.; Schubert, U. S.; Schneider, M.; Lehr, C. M. Impact of PEG and PEG-b-PAGE modified PLGA on nanoparticle formation, protein loading and release. *Int. J. Pharm.* **2016**, *500*, 187−195.
(80) Lee, H.; Dam, D.; Ha, J.; Yue, J.; Odom, T. Enhanced HER2 Degradation in Breast Cancer Cells by Lysosome-Targeting Gold Nanoconstructs. *ACS Nano* **2015**, *9*, 9859−9867.
(81) Friedman, L. M.; Rinon, A.; Schechter, B.; Lyass, L.; Lavi, S.; Bacus, S. S.; Sela, M.; Yarden, Y. Synergistic down-regulation of receptor tyrosine kinases by combinations of mAbs: Implications for cancer immunotherapy. *Proc. Natl. Acad. Sci. U. S. A.* **2005**, *102*, 1915−1920.
(82) Xu, S.; Olenyuk, B. Z.; Okamoto, C. T.; Hamm-Alvarez, S. F. Targeting receptor-mediated endocytotic pathways with nanoparticles: Rationale and advances. *Adv. Drug Delivery Rev.* **2013**, *65*, 121−138.
(83) Li, J. Y.; Perry, S. R.; Muniz-Medina, V.; Wang, X.; Wetzel, L. K.; Rebelatto, M. C.; Hinrichs, M. J. M.; Bezabeh, B. Z.; Fleming, R. L.; Dimasi, N.; Feng, H.; Toader, D.; Yuan, A. Q.; Xu, L.; Lin, J.; Gao, C.; Wu, H.; Dixit, R.; Osbourn, J. K.; Coats, S. R. A biparatopic HER2-targeting antibody-drug conjugate induces tumor regression in primary models refractory to or ineligible for HER2-targeted therapy. *Cancer Cell* **2016**, *29*, 117−129.
(84) Salomone, F.; Cardarelli, F.; Di Luca, M.; Boccardi, C.; Nifosì, R.; Bardi, G.; Di Bari, L.; Serresi, M.; Beltram, F. A novel chimeric cell-penetrating peptide with membrane-disruptive properties for efficient endosomal escape. *J. Controlled Release* **2012**, *163*, 293−303.
(85) Boeneman, K.; Delehanty, J. B.; Blanco-canosa, J. B.; Stewart, M. H.; Oh, E.; Huston, A. L.; Dawson, G.; Walters, R.; Domowicz, M.; Deschamps, J. R.; Algar, W. R.; Dimaggio, S.; Manono, J.; Spillmann, C. M.; Thompson, D.; Jennings, L.; Dawson, P. E.; Medintz, I. L. Selecting improved peptidyl motifs for cytosolic delivery of disparate protein and nanoparticle materials. *ACS Nano* **2013**, *7* (5), 1−33.
(86) O'Rourke, C.; Hopper, C.; MacRobert, A. J.; Phillips, J. B.; Woodhams, J. H. Could clinical photochemical internalisation be optimized to avoid neuronal toxicity? *Int. J. Pharm.* **2017**, *528* (1−2), 133−143.
(87) Helm, K.; Beyreis, M.; Mayr, C.; Ritter, M.; Jakab, M.; Kiesslich, T.; Plaetzer, K. In vitro cell death discrimination and screening method by simple and cost-effective viability analysis. *Cell. Physiol. Biochem.* **2017**, *41*, 1011−1019.
(88) Lai, P. S.; Lou, P. J.; Peng, C. L.; Pai, C. L.; Yen, W. N.; Huang, M. Y.; Young, T. H.; Shieh, M. J. Doxorubicin delivery by polyamidoamine dendrimer conjugation and photochemical internalization for cancer therapy. *J. Controlled Release* **2007**, *122*, 39−46.
(89) Cabral, H.; Nakanishi, M.; Kumagai, M.; Jang, W. D.; Nishiyama, N.; Kataoka, K. A photo-activated targeting chemotherapy using

DOI: 10.1021/acs.molpharmaceut.8b01318
Mol. Pharmaceutics 2019, 16, 1633−1647

glutathione sensitive camptothecin-loaded polymeric micelles. *Pharm. Res.* **2009**, *26*, 82−92.
(90) Wang, S.; Hüttmann, G.; Zhang, Z.; Vogel, A.; Birngruber, R.; Tangutoori, S.; Hasan, T.; Rahmanzadeh, R. Light-controlled delivery of monoclonal antibodies for targeted photoinactivation of Ki-67. *Mol. Pharmaceutics* **2015**, *12*, 3272−3281.
(91) Zhu, K.; Liu, G.; Hu, J.; Liu, S. Near-infrared light-activated photochemical internalization of reduction-responsive polyprodrug vesicles for synergistic photodynamic therapy and chemotherapy. *Biomacromolecules* **2017**, *18*, 2571−2582.
(92) Xu, P.; Gullotti, E.; Tong, L.; Highley, C. B.; Errabelli, D. R.; Hasan, T.; Cheng, J.-x.; Kohane, D. S.; Yeo, Y.; Martin, S.; Drive, J. Intracellular drug delivery by poly(lactic-co-glycolic acid) nanoparticles, revisited. *Mol. Pharmaceutics* **2009**, *6* (1), 190−201.
(93) Battelli, M. G.; Montacuti, V.; Stirpe, F. High sensitivity of cultured human trophoblasts to ribosome-inactivating proteins. *Exp. Cell Res.* **1992**, *201*, 109−112.
(94) Bergamaschi, G.; Perfetti, V.; Tonon, L.; Novella, A.; Lucotti, C.; Danova, M.; Glennie, M. J.; Merlini, G.; Cazzola, M. Saporin, a ribosome-inactivating protein used to prepare immunotoxins, induces cell death via apoptosis. *Br. J. Haematol.* **1996**, *93*, 789−794.
(95) Dai, L.; Liu, J.; Luo, Z.; Li, M.; Cai, K. Tumor therapy: targeted drug delivery systems. *J. Mater. Chem. B* **2016**, *4*, 6758−6772.
(96) Danhier, F.; Feron, O.; Préat, V. To exploit the tumor microenvironment: Passive and active tumor targeting of nanocarriers for anti-cancer drug delivery. *J. Controlled Release* **2010**, *148*, 135−146.
(97) Berg, K.; Nordstrand, S.; Selbo, P. K.; Tran, D. T. T.; Angell-Petersen, E.; Høgset, A. Disulfonated tetraphenyl chlorin (TPCS 2a), a novel photosensitizer developed for clinical utilization of photochemical internalization. *Photochemical and Photobiological Sciences* **2011**, *10*, 1637−1651.
(98) Zhu, W.; Okollie, B.; Artemov, D. Controlled internalization of Her-2/neu receptors by cross-linking for targeted delivery. *Cancer Biol. Ther.* **2007**, *6* (12), 1960−1966.
(99) Hapuarachchige, S.; Zhu, W.; Kato, Y.; Artemov, D. Bioorthogonal, two-component delivery systems based on antibody and drug-loaded nanocarriers for enhanced internalization of nanotherapeutics. *Biomaterials* **2014**, *35* (7), 2346−2354.
(100) Moody, P. R.; Sayers, E. J.; Magnusson, J. P.; Alexander, C.; Borri, P.; Watson, P.; Jones, A. T. Receptor crosslinking: A general method to trigger internalization and lysosomal targeting of therapeutic receptor:ligand complexes. *Mol. Ther.* **2015**, *23* (12), 1888−1898.
(101) Saraste, A. Morphologic Criteria and Detection of Apoptosis. *Herz* **1999**, *24* (3), 189−195.

DOI: 10.1021/acs.molpharmaceut.8b01318
Mol. Pharmaceutics 2019, 16, 1633−1647